**Atmospheric
Chemistry
and Physics**

Characterization of ambient aerosols in Mexico City during the MCMA-2003 campaign with Aerosol Mass Spectrometry: results from the CENICA Supersite

D. Salcedo[1,2], **T. B. Onasch**[3], **K. Dzepina**[2,4], **M. R. Canagaratna**[3], **Q. Zhang**[2,*], **J. A. Huffman**[2,4], **P. F. DeCarlo**[2,5], **J. T. Jayne**[3], **P. Mortimer**[3,**], **D. R. Worsnop**[3], **C. E. Kolb**[3], **K. S. Johnson**[6], **B. Zuberi**[6,***], **L. C. Marr**[6,****], **R. Volkamer**[6,*****], **L. T. Molina**[6,7], **M. J. Molina**[6,*****], **B. Cardenas**[8], **R. M. Bernabé**[8], **C. Márquez**[8], **J. S. Gaffney**[9], **N. A. Marley**[9], **A. Laskin**[10], **V. Shutthanandan**[10], **Y. Xie**[10], **W. Brune**[11], **R. Lesher**[11], **T. Shirley**[11], and **J. L. Jimenez**[2,4]

[1]Centro de Investigaciones Químicas, Universidad Autónoma del Estado de Morelos, Cuernavaca, Morelos, México
[2]Cooperative Institute for Research in the Environmental Sciences (CIRES), Univ. of Colorado at Boulder, Boulder, CO, USA
[3]Center for Aerosol and Cloud Chemistry, Aerodyne Research Inc., Billerica, MA, USA
[4]Department of Chemistry and Biochemistry, University of Colorado at Boulder, Boulder, CO, USA
[5]Program in Atmospheric and Oceanic Sciences, University of Colorado at Boulder, Boulder, CO, USA
[6]Department of Earth, Atmospheric and Planetary Sciences and Department of Chemistry, Massachusetts Institute of Technology, Cambridge, MA, USA
[7]Molina Center on Energy and Environment, CA, USA
[8]Centro Nacional de Investigación Capacitación Ambiental, Instituto Nacional de Ecología, México D.F., México
[9]Argonne National Laboratory, Argonne, IL, USA
[10]William R. Wiley Environmental Molecular Sciences Laboratory, Pacific Northwest National Lab., Richland, WA, USA
[11]Pennsylvania State University, University Park, PA, USA
*now at: Atmospheric Science Research Center, State University of New York-Albany, Albany, NY, USA
**now at: John Hopkins University, Baltimore, MD, USA
***now at: Department of Chemistry and Biochemistry, University of California San Diego, San Diego, CA, USA
****now at: GEO2 Technologies, Woburn, MA, USA
*****now at: Department of Civil and Environmental Engineering, Virginia Polytechnic Institute and State University, Blacksburg, VA, USA
******now at: Molina Center on Energy and Environment, CA, USA

Abstract. An Aerodyne Aerosol Mass Spectrometer (AMS) was deployed at the CENICA Supersite, during the Mexico City Metropolitan Area field study (MCMA-2003) from 31 March–4 May 2003 to investigate particle concentrations, sources, and processes. The AMS provides real time information on mass concentration and composition of the non-refractory species in particulate matter less than 1 μm (NR-PM$_1$) with high time and size-resolution. In order to account for the refractory material in the aerosol, we also present estimates of Black Carbon (BC) using an aethalometer and an estimate of the aerosol soil component obtained from Proton-Induced X-ray Emission Spectrometry (PIXE)

analysis of impactor substrates. Comparisons of AMS + BC + soil mass concentration with other collocated particle instruments (a LASAIR Optical Particle Counter, a PM$_{2.5}$ Tapered Element Oscillating Microbalance (TEOM), and a PM$_{2.5}$ DustTrak Aerosol Monitor) show that the AMS + BC + soil mass concentration is consistent with the total PM$_{2.5}$ mass concentration during MCMA-2003 within the combined uncertainties. In Mexico City, the organic fraction of the estimated PM$_{2.5}$ at CENICA represents, on average, 54.6% (standard deviation σ=10%) of the mass, with the rest consisting of inorganic compounds (mainly ammonium nitrate and sulfate/ammonium salts), BC, and soil. Inorganic compounds represent 27.5% of PM$_{2.5}$ (σ=10%); BC mass concentration is about 11% (σ=4%); while soil represents

Correspondence to: J. L. Jimenez
(jose.jimenez@colorado.edu)

about 6.9% (σ=4%). Size distributions are presented for the AMS species; they show an accumulation mode that contains mainly oxygenated organic and secondary inorganic compounds. The organic size distributions also contain a small organic particle mode that is likely indicative of fresh traffic emissions; small particle modes exist for the inorganic species as well. Evidence suggests that the organic and inorganic species are not always internally mixed, especially in the small modes. The aerosol seems to be neutralized most of the time; however, there were some periods when there was not enough ammonium to completely neutralize the nitrate, chloride and sulfate present. The diurnal cycle and size distributions of nitrate suggest local photochemical production. On the other hand, sulfate appears to be produced on a regional scale. There are indications of new particle formation and growth events when concentrations of SO_2 were high. Although the sources of chloride are not clear, this species seems to condense as ammonium chloride early in the morning and to evaporate as the temperature increases and RH decreases. The total and speciated mass concentrations and diurnal cycles measured during MCMA-2003 are similar to measurements during a previous field campaign at a nearby location.

1 Introduction

The Mexico City Metropolitan Area (MCMA) is one of the most highly populated cities in the world with 18 million people according to the 2000 census (INEGI, 2001). The MCMA is an elevated basin approximately 2240 meters above sea level, surrounded by mountains on the south, west and east. At this altitude, there is 23% less oxygen available than at sea level, which causes combustion to be less efficient (Molina and Molina, 2002). More than three million vehicles and more than five thousand industries emit more than 28 metric tons day^{-1} of particulate matter smaller than 10 μm (PM_{10}), including 17 tons day^{-1} of particulate matter smaller than 2.5 μm ($PM_{2.5}$), and 2400 tons day^{-1} of potential particle precursors such as SO_2, NO_x and organic compounds (see Table 1) (SMADF, 2002).

Because of the altitude and the subtropical latitude of the Mexico City basin, it receives intense solar radiation, which promotes the efficient formation of photochemical pollutants. According to official reports during 2001 and 2002, the ozone concentration exceeded the health-based standard (110 ppb for 1 h avg.) 70% of the days (SMADF, 2003). During the same years, the PM_{10} 24 h standard (150 μg m^{-3}) was exceeded one of every 12 days. In addition, the annual arithmetic mean PM_{10} standard (50 μg m^{-3}) was also exceeded during 2001 and 2002. Currently, there is no Mexican Standard for $PM_{2.5}$. Negative health effects due to air pollution in Mexico City have been reported (Calderon-Garciduenas et al., 2003), including specific effects associated with fine particles (Gold et al., 1999; Osornio-Vargas et al., 2003).

In addition to the visibility and health effects that air pollution in the Mexico City Valley causes on a local scale, pollution emitted in Mexico City can have effects on regional and global scales. Barth and Church (1999) studied the fate of the SO_2 emitted in Mexico City with a global model. According to these authors, most of the sulfur emitted in the city travels westward and northward, but small concentrations can be found as far northeast as the Mediterranean basin. According to these authors the average atmospheric lifetime of the sulfur emitted from Mexico City is 5.5 days, which is larger than the average lifetime of sulfur emitted in the rest of the world (3.9 days).

The Mexico City Metropolitan Area field experiment (MCMA-2003) was an intensive 5-week campaign that took place in the spring of 2003 (31 March–4 May), with the goal of investigating the atmospheric chemistry of the MCMA, with particular focus on emissions quantification, gas-phase photochemistry, and secondary PM formation. A focal point of the campaign was a highly instrumented "Supersite" located at the "Centro Nacional de Investigación y Capacitación Ambiental" (CENICA), in southeast Mexico City (see Fig. 1). During the MCMA-2003 campaign, we deployed an Aerodyne Quadrupole Aerosol Mass Spectrometer (Q-AMS) at CENICA. The AMS reports concentrations of non-refractory species in particles smaller than about 1 μm (NR-PM_1) with high time and size resolution (Jayne et al., 2000; Jimenez et al., 2003a). In order to account for the refractory aerosol material, we include in the analysis black carbon (BC) concentrations estimated with an aethalometer and an estimation of the aerosol soil component from Proton-Induced X-ray Emission Spectrometry (PIXE) analysis of impactor substrates.

Table 1. Daily emission rates of particles and potential particle precursors in the MCMA, which includes the Federal District and 18 municipalities in the State of Mexico (SMADF, 2002). SO_2 emissions are given in mass of SO_2; NO_x is reported as mass of NO_2; and organic compounds emissions are given as actual mass emitted. "Total organic compounds" refer to organic compounds emitted as gases and includes the "volatile organic compounds" (VOCs). Isoprene and monoterpenes are a fraction of the VOCs.

| Pollutant	(metric ton/day)
PM_{10}	28
$PM_{2.5}$	17
SO_2	40
NO_x	530
Total Organic Compounds	1829
Volatile Organic Compounds	1177
Isoprene and Monoterpenes	31

This paper describes the mass concentration time trends, chemical composition, and chemically-speciated size distributions observed at CENICA. The diurnal cycles and size distributions of the AMS components are discussed, as well as processes and sources of the AMS inorganic components. We compare results from MCMA-2003 with those published in a previous study of Mexico City aerosol and with data from the recently deployed citywide PM$_{2.5}$ monitoring network, both obtained at a site near CENICA (Cerro de la Estrella).

2 Experimental

2.1 Aerodyne Aerosol Mass Spectrometer (AMS)

The Q-AMS has been described in detail previously (Jayne et al., 2000; Jimenez et al., 2003a) so only a brief description will be given here. The AMS instrument consists of three main parts: an aerosol inlet, a particle sizing chamber, and a particle detection section. Particles are sampled from ambient pressure into ~1.5 Torr and are focused using an aerodynamic lens into a narrow beam of ~100 μm diameter (Heberlein et al., 2001). The aerodynamic lens has near unity transmission for particles in the size range of 60 nm to 600 nm, and partial transmission down to ~30 nm and up to ~1.5 μm (Jayne et al., 2000). In the expansion at the exit of the lens into the high vacuum chamber, the particles acquire a size-dependent velocity. The beam then passes through a spinning chopper wheel in the particle sizing chamber, where vacuum aerodynamic diameter (d_{va}) of the particles (Jimenez et al., 2003b, 2003c; DeCarlo et al., 2004) is determined by measuring the time it takes a particle to reach the detector (particle time-of-flight or P-ToF). In the detector, the particle beam impacts on a heated surface (~600°C) under high vacuum (~10^{-7} Torr), leading to flash vaporization of the "non-refractory" (NR) particle species. NR is defined operationally to include all species that evaporate in a few seconds under these conditions. In practice, NR includes species such as ammonium sulfate and bisulfate, ammonium chloride, ammonium nitrate, and organic compounds but excludes black carbon, crustal materials, and sea salt/sodium chloride. Non-refractory species internally mixed with refractory species (e.g., organics internally mixed with black carbon) can be quantitatively detected with the AMS (Katrib et al., 2004; Slowik et al., 2004). The NR particle species that are vaporized at the heated surface are then subjected to electron impact (EI) ionization, which forms positive ions that are analyzed with a quadrupole mass spectrometer. The signal is linear with particle mass of a given species and detection limits below 1 μg m^{-3} are typically achieved for all species (see below).

During the MCMA-2003 campaign, a recently developed beam width probe (BWP) was used with the AMS to provide a continuous measurement of surrogate particle morphology
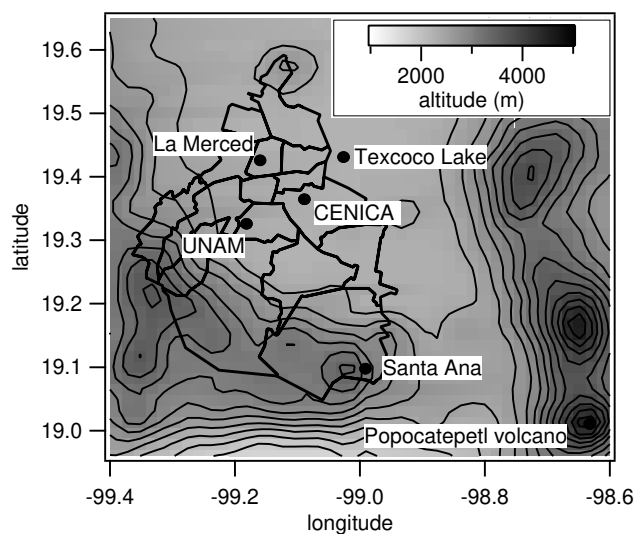
Fig. 1. Topographical map of the Mexico City Metropolitan Area and surrounding region. The division and limits of the Federal District are shown.

(non-sphericity) and to allow the estimation of the potentially reduced particle collection efficiency due to particle shape (Huffman et al., 2005). The probe used in this study consisted of a 0.41 mm diameter wire, which was moved intermittently to a fixed position blocking part of the particle beam near the AMS vaporizer in order to determine the attenuation of the signal vs. wire position. The BWP was alternated between the "out" position (not blocking any part of the vaporizer) and one of seven partially blocking positions in front of the vaporizer. The various BWP blocked positions and the unblocked position were alternated every two minutes. This produced a 4-min, 50% duty cycle dataset without the BWP that is used to derive particle concentrations in this paper. The details of the operation of the BWP during MCMA-2003 as well as the results obtained with it are discussed in detail elsewhere (Salcedo et al., 2005).

The AMS was located inside a hut built on the roof of the 12 m tall building that houses CENICA. Ambient air was sampled at a flow rate of 9 lpm through a PM$_{2.5}$ cyclone (URG-2000-30EN, URG, Chapel Hill, NC) located 2.3 m above the roof of the hut and drawn into 9.525 mm (3/8 inch) copper tubing to within 15 cm of the AMS inlet, where 8.9 lpm were exhausted by a vacuum pump and ~0.1 lpm was sampled into the AMS from the center of the 9.525 mm line. The total length of the inlet line was 5.3 m. Maximum particle losses due to diffusion and bends in the line were calculated (Baron and Willeke, 2001) to be 6.5% for 30 nm particles and 0.7% for 1 μm particles.

The ionization efficiency (IE) of the AMS was calibrated every few days with dry monodisperse NH$_4$NO$_3$ particles with the procedure described previously (Jimenez et al., 2003a; Zhang et al., 2005b). Results of all IE calibrations

for the CENICA AMS during the campaign are shown in Fig. S1 of the supplementary material (http://www.atmos-chem-phys.net/6/925/acp-6-925-sp.pdf). The figure shows that the AMS was consistently stable during the campaign.

The correlation between the time series of the main ion fragments used (in MS mode) to calculate the mass concentration of each one of the inorganic species during the MCMA-2003 study is shown in Fig. S2 in the supplementary information (http://www.atmos-chem-phys.net/6/925/acp-6-925-sp.pdf). Although there is some scatter in the individual plots, likely owing to limited signal-to-noise of the individual measurements, deviations from linearity are small. This indicates that unsubtracted interferences from organic fragments in the retrieved concentrations of the inorganic species are not significant during this campaign and lends confidence to the derived chemically-speciated size distributions.

The ions chosen and the main species monitored with the AMS P-ToF mode during this campaign were: m/z 16 for ammonium (NH_2^+); m/z 18 for water (H_2O^+); m/z 28 for the airbeam (N_2^+); m/z 30 and 46 for nitrate (NO^+, NO_2^+); m/z 36 for chloride (HCl^+); m/z 48 and 64 for sulfate (SO^+, SO_2^+); m/z 43, 44, 55, 57, 67, 77, and 141 for organic species; and m/z 202 and 226 for polycyclic aromatic hydrocarbons (PAHs).

The MCMA data were analyzed using previously published relative ionization efficiencies (RIEs) of 1.2 for sulfate, 1.1 for nitrate, 1.4 for organics and 1.3 for chloride (Jimenez et al., 2003a; Alfarra et al., 2004). The NH_4NO_3 IE calibration allows for the direct determination of the ammonium RIE. The ammonium RIE measured for the CENICA AMS ranged from 3.8 to 6.2.

The detection limits (DLs) from individual species were determined by analyzing periods in which ambient filtered air was sampled and are reported as three times the standard deviation (3σ) of the reported mass concentration during those periods. DLs during this campaign for the CENICA AMS were 0.01, 0.09, 0.11, 0.41 and 0.04 μg m^{-3} for nitrate, sulfate, ammonium, organics and chloride respectively for a 10 min. averaging time. These DLs are similar to those reported for previous Q-AMS campaigns (Zhang et al., 2005b).

AMS Collection Efficiencies (CE) observed in previous studies range from 0.43 to 1 (Allan et al., 2004; Drewnick et al., 2004a; Hogrefe et al., 2004; Zhang et al., 2005b). This CE has three contributions: $CE=E_L * E_s * E_b$ (Huffman et al., 2005). The E_L term accounts for the portion of PM$_{2.5}$ that is not transmitted into the AMS due to the approximate PM$_1$ size cut (Jayne et al., 2000; Zhang et al., 2005b) of the aerodynamic lens in the AMS. In principle, the shape-related collection efficiency (E_s) could be less than one for nonspherical particles because the efficiency with which they are focused by the lens is reduced (Jayne et al., 2000; Huffman et al., 2005) and this in turn could potentially cause irregular particles to "miss" the AMS vaporizer. The bounce-related collection efficiency (E_b) could be smaller than one

if some dry, less-volatile particles such as those with a high proportion of $(NH_4)_2SO_4$, bounce after impacting the AMS vaporizer, instead of evaporating. Previously, the latter two effects (and sometimes all three effects) had been lumped in one collection efficiency ($CE=E_s * E_b$) (Alfarra et al., 2004; Drewnick et al., 2004b; Zhang et al., 2005b). The newly developed beam width probe (BWP) that was operated in this campaign showed that $E_s \sim 1$ during this field campaign (Salcedo et al., 2005). E_b is more difficult to determine because it likely depends on particle phase (liquid vs. solid), water content, and particle composition. Particles with significant ammonium sulfate content appear to bounce with $E_b \sim 0.5$ when they are dry inside the AMS, and to be collected with $E_b \sim 1$ when they retain water after entering the vacuum system (Allan et al., 2004). Pure ammonium nitrate and ammonium nitrate-dominated ambient particles are collected with $E_b \sim 1$ (Jayne et al., 2000). The evidence is less clear for organic-dominated particles, as was the case during most of the MCMA-2003 campaign. Chamber experiments have shown that secondary organic aerosols (SOA) formed from photooxidation of aromatics, and from ozonolysis of biogenic compounds have an $E_b \sim 0.5$ (Bahreini et al., 2005). Since analysis of the submicron aerosol in Mexico City shows that a large fraction is oxygenated organics (OOA), a similar value should be applicable to this study. We did not experimentally determine E_b during MCMA 2003; however, given the evidence and uncertainties from previous laboratory studies and field campaigns, plus the evidence of internal mixing for most species and most of the campaign, we have applied a value of $E_b=0.5$ for all species for this campaign. We estimate the maximum range of possible values of this parameter between about 0.45 and 0.70. Thus the mass concentrations reported in this paper have a range of uncertainty of about -30% and $+10\%$ due to the uncertainty in particle collection efficiency. The comparisons with other instruments presented in Sect. 3.1 are consistent with the value of CE chosen here. Despite the uncertainty in the absolute concentrations, the relative variation in concentrations and size distributions reported here have a lower uncertainty, as evidenced by the fact that the dynamics of the AMS and TEOM/DustTrak concentrations track each other during the campaign (see Sect. 3.1).

All mass concentrations presented in this paper for all instruments are at ambient temperature and pressure conditions (local pressure is approximately 76 kPa). Local Standard Time in Mexico City normally corresponds to Central Standard Time (CST) or Coordinated Universal Time (UTC) minus 6 h. On 6 April 2003 at 2:00 AM the Daylight Savings Time period started in Mexico; after that, local time corresponded to Central Daylight Saving Time (CDT) or UTC minus 5 h. All data in this paper is reported in Local Time, i.e. CST before 6 April and CDT after 6 April.

2.2 Black carbon measurements

The black carbon content of fine aerosols was estimated from the aerosol light absorption using a seven-channel aethalometer (RTAA-1000, Magee Scientific, Berkeley, CA). Its sampling line was found to effectively collect aerosols in the 0.1 to 2.0 micron size range (PM_2). The particles are collected within the instrument by continuous filtration through a quartz filter tape strip. The optical transmission of the deposited aerosol particles is then measured sequentially at seven wavelengths (370, 450, 520, 590, 660, 880, and 950 nm). Black carbon is a strongly absorbing component whose light absorption coefficient is relatively constant over a broad spectral region. The instrument automatically estimates the black carbon concentration from the transmission measurements by assuming black carbon to be the main absorbing aerosol species in the samples with a mass specific absorption coefficient of 19 m^2 g^{-1} (Hansen et al., 1982; Marley et al., 2001). This value is larger than those typically used for the absorption of black carbon suspended in air due to the enhancement of the particle absorption in the fiber matrix of the filter tape (A. Hansen, Magee Scientific, personal communication). Data were recorded for each of the seven channels at a two-minute time resolution. In addition, the analog output of the 520 nm channel was monitored continuously and one minute averages of this channel were recorded separately. As the sample is deposited on the paper tape strip, the light attenuation steadily increases. At high sample loadings the high absorptions cause sensitivity to decrease. To prevent this, the instrument automatically advances the tape to a new sample spot when light attenuation becomes severe. The instrument sample was diluted 10:1 to minimize the instrument down time created by too frequent tape advances due to the high black carbon loading observed in Mexico City.

Unlike other absorbing aerosol species (e.g. humic like substances), black carbon absorption is relatively constant from the ultraviolet to the infrared (Marley et al., 2001). Thus a comparison of results from the different channels can act as an independent validation of the assumption that black carbon is the main absorbing species in the samples. For the sampling period, all seven channels were found to be in excellent agreement, with a variation of 1–2%, indicating that black carbon was indeed the major light absorbing material present in the aerosol, if not the only one. Since results obtained at shorter wavelengths may include contributions from other absorbing aerosols such as organic carbon compounds, results from the 880 nm channel were used in this study (Hansen et al., 1982).

2.3 Impactor aerosol collection and PIXE analysis

A detailed description of the impactor sampling and analysis techniques are given elsewhere (Johnson et al., 2006; Shutthanandan et al., 2002), hence only a brief description

is presented here. Impactor aerosol collections were made continuously onto Teflon strips with a 3-Stage IMPROVE DRUM impactor (UC Davis, California) in size ranges 1.15–2.5 μm, 0.34–1.15 μm, and 0.07–0.34 μm. The DRUM was operated with a fixed flow rate of 10 SLPM and rotation of 2 mm per 12 h. Proton-Induced X-ray Emission (PIXE) samples were analyzed within several weeks following the campaign at the Environmental Molecular Sciences Laboratory (EMSL), a national scientific facility within Pacific Northwest National Laboratory located in Richland, WA. A 3.5 MeV proton beam with diameter 0.5 mm was used during analysis. PIXE spectra were interpreted with the GUPIX program (Maxwell et al., 1995) and concentrations of elements Na to Pb determined by calibration to known standards. Concentrations are given in 6-h averages.

The soil particulate mass concentration is estimated from PIXE mass concentrations using the method described by Malm et al. (1994). These authors estimate the soil particulate mass concentration by summing the elements predominantly associated with soil, plus oxygen for the most common oxides (Al_2O_3, SiO_2, CaO, FeO, Fe_2O_3, TiO_2), plus corrections for other compounds such as K_2O, MgO, Na_2O, water and carbonate. The equation used is:

$$[\text{soil}] = 2.20[\text{Al}] + 2.49[\text{Si}] + 1.63[\text{Ca}] + 2.42[\text{Fe}] + 1.94[\text{Ti}] \tag{1}$$

2.4 Total PM instrumentation

In addition to the instruments described above, three other particle instruments were deployed at CENICA: a LASAIR Optical Particle Counter model 1001 (Particle Measuring Systems, Boulder, CO); a DustTrak Aerosol Monitor model 8520 (TSI, St. Paul, MN); and a Tapered Element Oscillating Microbalance (TEOM, Rupprecht & Patashnick, East Greenbush, NY).

The LASAIR device detects light scattered by individual particles crossing a detection volume illuminated with laser light. The LASAIR was calibrated for this campaign using 100–1000 nm polystyrene latex (PSL) spheres and reports the number concentration of particles in 8 different size channels (0.1–0.2 μm, 0.2–0.3 μm, 0.3–0.4 μm, 0.4–05 μm, 0.5–0.7 μm, 0.7–1.0 μm, 1.0–2.0 μm, 2.0–5.0 μm; equivalent geometric diameter, d_p). The nominal detection efficiency is 100% for all channels, with the exception of 50% for the smallest channel. The maximum ambient concentration recommended for the LASAIR 1001 is 353 cm^{-3}, however, the system was operated during MCMA-2003 with high ambient particle concentrations without a dilution system. This very likely caused the instrument to undercount particles due to coincidence in the sampling volume. A similar effect has been observed in other studies (Murphy et al., 1997). Another possible effect of the LASAIR operating under saturation conditions is a shift in the size distribution to larger sizes
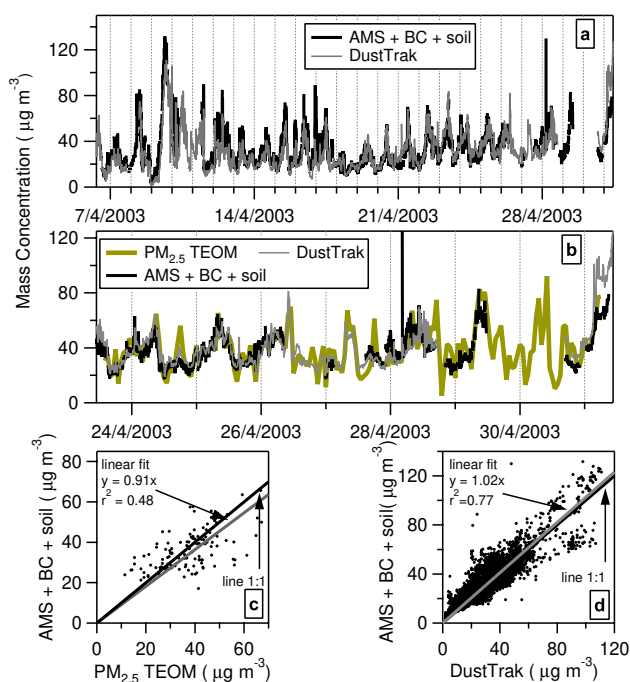
Fig. 2. Panels **a** and **b**: comparison of the time series of the AMS + BC + soil with DustTrak and TEOM PM$_{2.5}$ mass concentrations. Panels **c** and **d**: scatter plots and linear fits for the above comparisons. TEOM PM$_{2.5}$ data in panels b and c, has a resolution of 1 h; AMS + BC + soil data in panel c was averaged in 1 h periods. Grey lines are linear fits to the data. Lines 1:1 are shown in black as reference.

because the instrument may classify multiple particles in the sensing volume as a single larger particle.

The DustTrak is an aerosol photometer that uses a laser-beam to illuminate a sample stream, in which multiple particles scatter light in all directions. A detector determines the total amount of light scattered at a 90 degree angle, which is roughly proportional to the mass concentration of the aerosol (TSI, 2004). The DustTrak deployed during the MCMA campaign used a PM$_{2.5}$ impactor inlet. The Dust-Trak was calibrated with gravimetric filter measurements taken by CENICA during the MCMA-2003 campaign and agreed within 5% with a similar unit on board the Aerodyne Mobile Lab when parked at CENICA.

The TEOM measures the PM$_{2.5}$ total mass concentration using a vibrating element, whose resonant frequency depends on the accumulated particle mass collected on a filter located at the extreme of the element (Hinds, 1999). The TEOM used during the MCMA-2003 operated at 35°C and was not equipped with a Sample Equilibration System (SES).

3 Results and discussion

3.1 Comparison between speciated and total PM measurements

Using the instruments described in the experimental section, a closure study of the chemical composition of the MCMA-2003 average aerosol is presented here. The DustTrak and TEOM measure the total particulate mass concentration, including both refractory and non-refractory species. The sum of the AMS, BC, and estimated soil particulate mass concentrations represents individual measurements of the speciated non-refractory and refractory components of the total PM$_{2.5}$. PIXE analyses on the impactor substrates indicate that the average concentration of NaCl was at most 0.1 μg m^{-3}, and hence we did not include sodium in the correction of NR-PM$_1$. Another species that we did not include is particulate water, because there are significant uncertainties in water quantification with the AMS due to evaporation losses in the inlet. Note that, although water evaporation in the AMS inlet has been observed by several groups, evaporation of other species is not believed to be a problem for AMS ambient measurements, since the vapor pressure of other aerosol components is typically at least 6–7 orders of magnitude below that of water. The addition of BC and soil to the AMS data is important for the comparison with total PM instruments because the BC + soil mass concentration was equivalent to 20% of the NR-PM$_1$ during the MCMA-2003 (see below).

Panels a and b of Fig. 2 compare AMS + BC + soil mass concentration with PM$_{2.5}$ mass concentration measured by the DustTrak and TEOM. For the TEOM only a few days at the end of the campaign were available due to instrument malfunction in the earlier part. Scatter plots between the three data sets are also shown in Fig. 2, panels c and d. Note that the AMS measured approximately PM$_1$, while the aethalometer determined PM$_2$ BC, and the impactor substrates collected PM$_{2.5}$. On average, the total AMS + BC + soil concentrations are within 20% of the total PM$_{2.5}$ mass measured by either TEOM or DustTrak. The agreement between AMS + BC + soil concentrations and the other total mass measurements suggests the majority of non-refractory mass is found in particles <1 μm. These observations can be further substantiated by analyzing the size distribution data provided by the LASAIR.

The size distributions of the LASAIR measurements and the combined AMS + BC + soil mass loadings are compared in Fig. 3 (note the different scales). The black carbon size distribution was estimated using the size distribution of ion fragment m/z 57, which has been used as a marker for fresh primary emitted particles; thus, it is expected to have a similar size distribution as black carbon (Zhang et al., 2005a, 2005c). The size distribution of AMS fragment m/z 57 was scaled so that the integrated mass concentration was equal to the BC mass concentration. The number concentration of
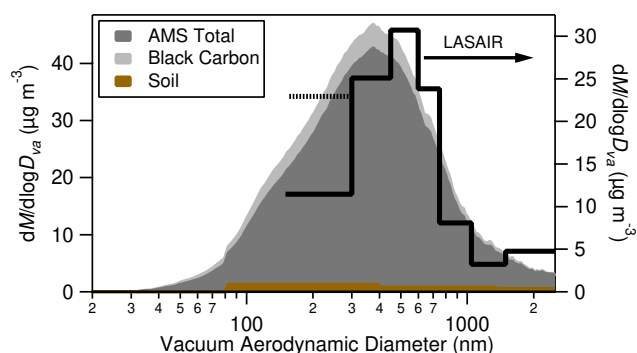
Fig. 3. Comparison of the (AMS + estimated BC + soil) and LA-SAIR size distributions. The BC, AMS and soil size distributions are stacked. The dashed line represents the mass concentration of the smallest LASAIR size channel multiplied by two in order to account for the 50% collection efficiency in this channel.

Fig. 4. Average mass composition of $PM_{2.5}$ (approximated as AMS + BC + soil) for the MCMA-2003 campaign. Average was made over all times periods where data from the three measurements were available.

particles in each LASAIR channel was converted to volume concentration assuming that the particle probability density is constant for all sizes in each bin. Then, we converted the particle volume concentration into mass concentration by multiplying the volume by the estimated size dependent material density (ρ_m, g cm^{-3}), calculated using the following equation (DeCarlo et al., 2004):

$$\rho_m = \frac{[NO_3^-] + [SO_4^{2-}] + [NH_4^+] + [Cl^-] + [\text{organics}] + [BC] + [\text{soil}]}{\frac{[NO_3^-]+[SO_4^{2-}]+[NH_4^+]}{1.75} + \frac{[Cl^-]}{1.52} + \frac{[\text{organics}]}{1.2} + \frac{[BC]}{1.77} + \frac{[\text{soil}]}{2.7}}$$

(2)

where $[NO_3^-]$, $[SO_4^{2-}]$, $[NH_4^+]$, $[Cl^-]$, [organics], [BC], and [soil] represent the size dependent mass concentration of each species. Equation (2) assumes that the densities of ammonium nitrate, ammonium sulfate, and ammonium bisulfate are approximately 1.75 g cm^3 (Lide, 1991); the density of ammonium chloride is 1.52 g cm^{-3} (Lide, 1991); the density of organics is 1.2 g cm^3 (Turpin and Lim, 2001); the density of black carbon 1.77 g cm^{-3} (Park et al., 2004); the average density of soil, calculated from the weighted average density of the main oxides (Lide, 1991), is 2.7 g cm^{-3}. The d_{va} corresponding to the geometric diameter (d_p) of each channel boundary of the LASAIR and the impactor substrates, was also calculated from d_p using the estimated size-dependent density (DeCarlo et al., 2004).

Figure 3 shows that the LASAIR measured lower mass concentrations than the AMS + BC + soil, which is explained by the fact that the instrument was operating under saturated counting conditions (see Sect. 2.4). The shapes of the size distributions in Fig. 3 are similar for large particle sizes, while the LASAIR detects fewer small particles than the AMS + BC + soil. This may partially be due to the larger size cut at the small end for the LASAIR, that nominally detects 50% of the particles between d_p=100–200 nm, compared to the AMS, which detects a significant fraction of
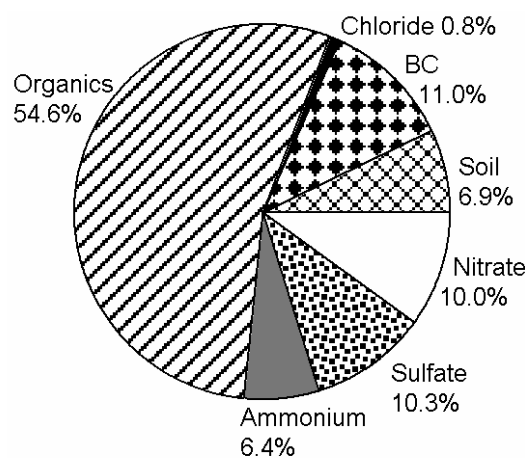
(spherical) particles down to about 60 nm and has some transmission down to ∼33 nm (Zhang et al., 2004). The agreement between the size distributions can be improved if the mass concentration in the smallest LASAIR channel is multiplied by two in order to account for the lower detection efficiency of the smallest particles, as it is shown by the dashed line in Fig. 3. Another possible source for the apparent discrepancy at low particle sizes is the presence of irregular soot particles that are sized smaller than their volume-equivalent diameter by the AMS (DeCarlo et al., 2004; Slowik et al., 2004; Zhang et al., 2005b) and likely sized larger by the LA-SAIR since light scattering is roughly proportional to particle surface area. A similar apparent discrepancy when comparing AMS and SMPS data for Pittsburgh is shown in Fig. 4a of Zhang et al. (2005b).

In spite of the saturation effects on the LASAIR data, Fig. 3 provides an important piece of information: the mass concentration of particles between 1 and 3 μm is only 7% of the mass concentration in the size range 0.15–3 μm (even when the LASAIR size distribution might be shifted to larger sizes due to the reasons mentioned above). In some previous AMS studies the concentrations of particles in this size range have been relatively high, leading to significantly higher $PM_{2.5}$ than PM_1 mass concentrations (Zhang et al., 2005b). The fact that this is not the case during MCMA-2003 is consistent with the agreement seen in Fig. 2 between the total AMS + BC + soil concentrations and those measured by the TEOM and DustTrak which operated with $PM_{2.5}$ size cuts. In conclusion, the combination of the AMS, BC, and soil particulate mass measurements can be used as an estimate of $PM_{2.5}$ during MCMA-2003.

Table 2. Summary of the AMS, BC, and soil mass concentration data during the MCMA-2003 campaign. Averages are made over the complete time interval where data is available. The averaging time interval is different for NR-PM$_1$, BC and soil (see Fig. 5).

Species	Average (μg m^{-3})	Std. Dev. (μg m^{-3})	Minimum (μg m^{-3})	Maximum (μg m^{-3})
Nitrate	3.7	5.1	0.1	49.0
Sulfate	3.1	2.3	below DL	22.7
Ammonium	2.2	1.6	below DL	14.8
Chloride	0.3	0.7	below DL	26.3
Organics	21.6	14.8	1.3	106.5
Total NR-PM$_1$	30.9	19.0	1.7	125.0
Black Carbon	3.4	2.5	0.2	52.7
Soil	2.1	0.7	1.1	4.6

3.2 Average aerosol mass concentration and composition

The average mass concentrations of AMS + BC + soil during the entire measurement period are presented in Fig. 4 and Table 2. Organic species represent the main component of estimated PM$_{2.5}$ with 54.6% (standard deviation, σ=10%) of the total mass concentration. Inorganic species represent 27.5% (σ=10%), with sulfate and nitrate being the most abundant components with 10.0% (σ=7%) and 10.3% (σ=6%) respectively of the total mass. Ammonium and chloride contribute to the average mass with 6.4% (σ=3%) and 0.8% (σ=1%), respectively. The BC mass concentration is 11.0% (σ=4%) of the PM$_{2.5}$ mass, while soil represents 6.9% (σ=4%).

Compared with AMS measurements in other cities, the average total NR-PM$_1$ mass concentration in the MCMA (40.7 μg m^{-3} at STP, 1 atm and 298 K) is substantially larger than the average concentrations measured in Pittsburgh in September 2002 and New York City in July 2001 with an AMS: 14.8 μg m^{-3} (Zhang et al., 2005b) and 8.8 μg m^{-3} (Drewnick et al., 2004b) respectively. Also, the PM composition is different. While the largest component of NR-PM$_1$ in the MCMA is by far the organic matter, in Pittsburgh and New York City the major component is sulfate with 47% and 45% of the NR-PM$_1$ mass, respectively. Organic matter accounts for 30% of the mass in both cities. Nitrate represents only 6% and 9% of the NR-PM$_1$ mass in Pittsburgh and New York, respectively, which is slightly lower than its fraction in Mexico City. 17% of the NR-PM$_1$ in Pittsburgh and 16% in New York City is ammonium, which is larger than in Mexico due to the much larger sulfate fraction in those two cities.

3.3 Time variations and diurnal cycles of the aerosol species

Figure 5a–c shows the time series of the speciated mass concentration of NR-PM$_1$ from 3 April to 5 May 2003, mea-

sured at CENICA with the AMS. The "NR Total" concentration is defined as the sum of all the AMS-measured NR species (nitrate, sulfate, ammonium, chloride and organics). We also show the time series of BC and soil in panels d and e of the figure. Finally, in panel f, we show the fractional species mass contribution for the estimated PM$_{2.5}$. The organic species show a clear diurnal cycle, as do nitrate and black carbon. The ammonium concentration follows the nitrate and sulfate concentrations in time (see Sect. 3.5), which suggests that these three species exist mainly in the forms of NH$_4$NO$_3$, and sulfate-ammonium salts (ammonium sulfate, bisulfate, and/or letovicite (Schlenker et al., 2004)). Chloride is generally present at very low concentrations, but some very large short-lived spikes (up to 26.3 μg m^{-3}) are observed throughout the campaign. Finally the soil concentration is remarkably constant during the campaign, indicating that the nature of its sources is different from the rest of the components.

Since vehicle traffic is one of the main sources of particles and particle precursors in the MCMA (SMADF, 2002), it is expected that traffic patterns have an important effect on the observed particle concentrations. Time periods which are expected to have different traffic patterns are identified in Fig. 5. In Mexico City, weekends are expected to have different traffic patterns from weekdays due to the "Hoy no circula" (HNC, "Not driving today") program which limits a fraction of the cars from driving on one day depending on the last digit of the car's license plate. The driving restriction applies to cars older than 10 years and/or to those that do not comply with the emission standards. The HNC program is enforced on weekdays but not on weekends. During MCMA-2003 a traffic count that was obtained on one of the main avenues connecting the south of the city to downtown (Avenida Insurgentes Sur), showed that there is a small reduction in traffic on Saturday with respect to weekdays ($\sim$5%); on Sunday the reduction in traffic is more noticeable ($\sim$25%). These average traffic counts did not show any significant reductions during school vacation week (16 to 25 April), but during Holy weekend (19 to 21 April), which is one of the most popular vacation periods in the MCMA, a considerable traffic reduction was observed ($\sim$30%). We did not attempt to correlate these traffic counts with particle data obtained at CENICA because the sites are several kilometers apart and because the large volume of traffic at this central location may have saturated the traffic volume capacity some of the time, and may not fully represent the variability of the traffic volume on the entire city. However, a qualitative comparison shows that the average AMS + BC + soil concentration during Friday and Saturday of the holy weekend were among the lowest in the campaign (PM concentrations were 45% lower than average concentration on other Fridays and Saturdays), as expected from a significant reduction in traffic that caused lower vehicle emissions of primary particles and particle precursors such as NO$_x$ and organic compounds. Concentrations of AMS + BC + soil decrease $\sim$20% on Sundays
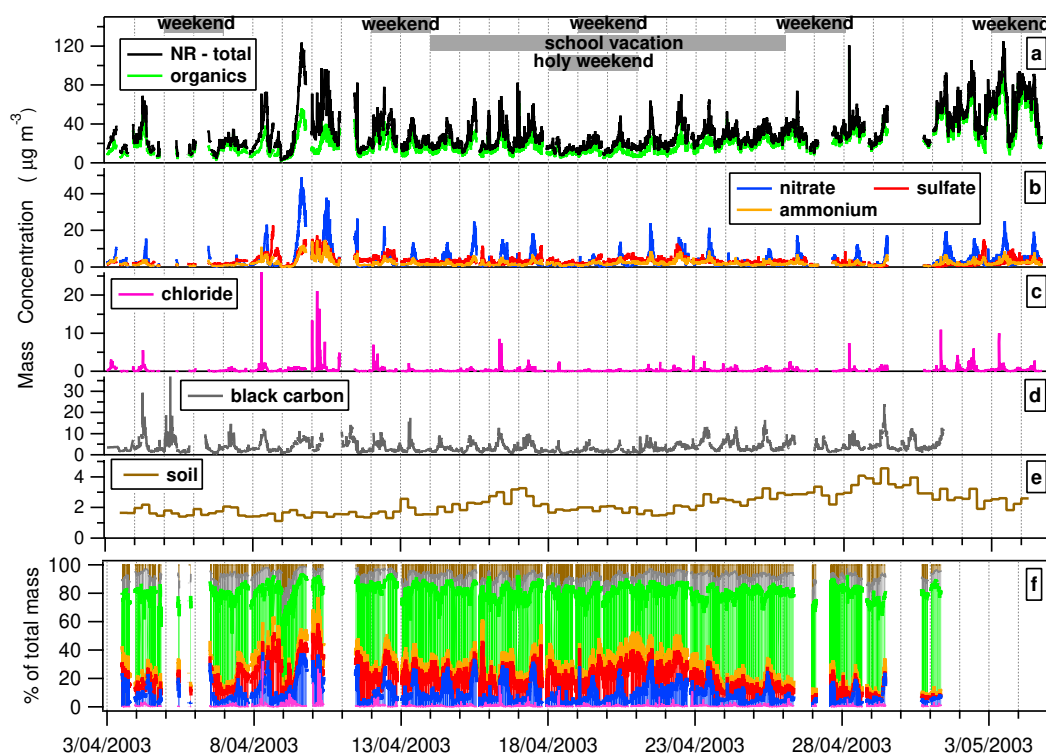
Fig. 5. Panels **a–e**. Time series of the mass concentration of the AMS NR-PM$_1$ species (NR-Total = nitrate + sulfate + ammonium + chloride + organics), aethalometer BC, and estimated soil at the CENICA Supersite. Panel **f**: Time series of the percent mass composition of Total AMS + BC + soil.

as would also be expected from a reduction in traffic. However, AMS + BC + soil increase ~20% during Saturdays. A possible explanation for the increase in particle mass on Saturdays is that, even when the number of vehicles decrease, the fraction of older and more polluting cars circulating in the city increases because the HNC program is not enforced.

While traffic patterns may explain some of the trends in aerosol loadings, they do not explain features such as the high aerosol concentrations on 9–11 April. Meteorology must also be taken into account to understand the observed dynamics of particle concentrations and properties. A review of the meteorology in Mexico City during the MCMA-2003 campaign is presented by de Foy et al. (2005), who discuss the fact that synoptic weather patterns, regional land-sea breezes, and local thermally driven flows influenced by the mountains combine to produce very complex meteorological patterns. According to de Foy et al. (2005), 9 to 11 April corresponded to "Cold Surge" days which were influenced by the arrival of a cold air mass that caused reduced vertical mixing in the morning and a lower boundary layer height throughout the day, which favored the accumulation of pollutants. Despite the cloudiness on April 9th, intense photochemical activity (evidenced by uniform O$_3$ levels over most of the eastern part of the Mexico City valley, (de Foy et al., 2005)) combined with reduced dilution led to the highest NR-PM$_1$ con-

centrations observed during MCMA-2003. According to de Foy et al. (2005), on 10 April, a large SO$_2$ plume covered the northern half of the city, with maximum concentrations of 277 ppb, which might explain the large concentrations of sulfate observed in the NR-PM$_1$. 11 April which also had the highest CO concentrations during the campaign, presented one of the strongest surface inversions.

Figure 5a shows an increase in aerosol organic fraction during the second half of the campaign. One possible reason for this is the impact of biomass burning in Central and Southern Mexico which steadily increased from mid-April according to satellite fire counts (C. Wiedinmyer, NCAR, and B. de Foy, UCSD, personal communications). The plumes from these fires appear to have been transported to the vicinity of Mexico City during this period according to satellite data, an issue which is being further investigated (S. Massie, NCAR, and B. de Foy, USCD, personal communications).

The average diurnal cycles of all the species are shown in Figs. 6a–e, g, and h. Panel f compares the diurnal cycle of the organics mass concentration with the diurnal cycle of ion fragments m/z 44 and 57, which are markers for oxygenated (OOA) and hydrocarbon-like (HOA) organics, respectively (Zhang et al., 2005a, c). Figure 6 shows that nitrate has a very sharp diurnal pattern with a maximum at midday.
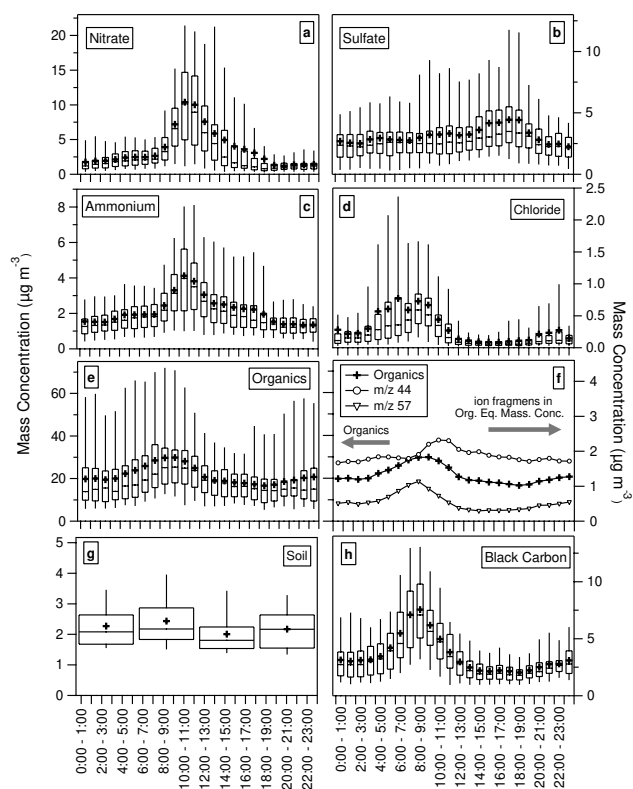
Fig. 6. Panels **a–e**: box-whisker plots of the diurnal cycles of the mass concentration of AMS species. Crosses represent the average mass concentration; horizontal lines represent the median; bottom and top of the boxes represent the 25 and 75% limits respectively; and the bottom and the top whiskers represent the 5 and 95% limits respectively. Panel **f**: average diurnal cycles of AMS organics mass concentration, and AMS fragments m/z 44 (marker for oxygenated organics) and m/z 57 (marker for hydrocarbon-like organics) in Org. Eq. Mass Concentration. Panel **g–h**: box-whisker plots of the diurnal cycles of soil and BC mass concentration. Averages are made over the complete time interval where data is available. The average time interval is different for NR-PM$_1$, BC and soil (see Fig. 5).

We attribute this behavior to nitric acid being formed photochemically during the day from the reaction of NO$_2$ and OH; the acid reacts with ammonia to form ammonium nitrate on preexisting particles (see Sect. 3.6). Thus, ammonium has a diurnal cycle that is very similar to that of nitrate. However, the ammonium concentrations at times other than midday are not as low as the nitrate concentrations. This is because at these times a significant fraction of the particulate ammonium is in the form of sulfate-ammonium salts (see Sect. 3.5). The diurnal pattern of sulfate does not vary as much as that of nitrate, remaining around 2–3 μg m^{-3} most of the time, which is explained by a more regional production from the oxidation of SO$_2$ (see Sect. 3.6), and possibly some larger-scale transport. Black carbon is primarily emitted by combustion sources and, as expected, its diurnal cycle has a peak early in the morning during the rush hour. At mid-

day, the concentration of BC decreases because the boundary layer rises causing a dilution of the accumulated BC that is much faster than the rate of emission at that time. Chloride shows the largest concentrations during the morning hours probably because it exists as ammonium chloride, which is a volatile compound that evaporates as the temperature increases and the humidity decreases during the morning (see Sect. 3.8). Figure 6f suggests that the organic diurnal pattern is a combination of traffic emissions in the morning (represented by fragment m/z 57) and photochemical production of secondary organic aerosol during sunlit hours (related to fragment m/z 44).
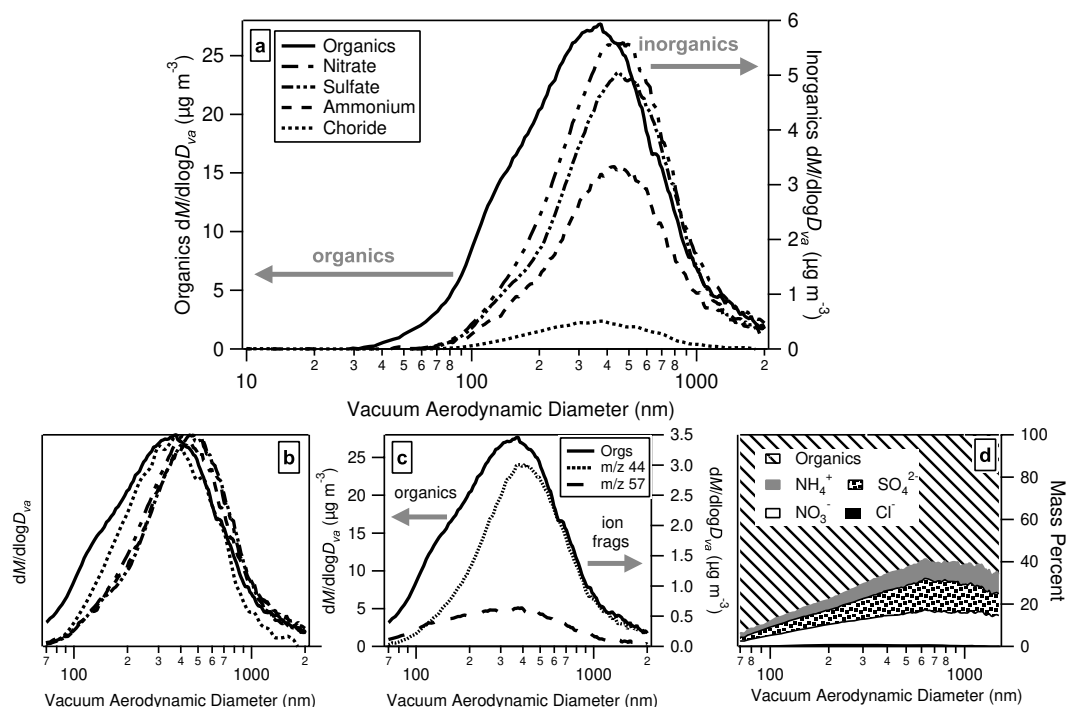
3.4   Size distribution of NR-PM$_1$

The average size distributions of the NR-PM$_1$ species for the whole campaign are shown in Fig. 7a. Figure 7b shows all the size distributions scaled to the same maximum in order to compare their relative shapes. Figure 7c compares the average size distribution of the organics with the size distributions of AMS fragments m/z 44 and m/z 57. Figure 7d presents the percent composition of the NR-total mass concentration as a function of particle size. Figure 7 shows that the accumulation mode dominates the average size distribution for most species. Figure 7b shows that sulfate, nitrate and ammonium have a very similar size distribution, while the size distribution of organics is much broader. The organic size distribution presents a shoulder at small sizes and chloride shows an intermediate size distribution between those of organics and the other inorganics.

In order to determine the mode diameters and widths of the size distributions shown in Fig. 7a, they were fitted to log-normal modes of the form:

$$\frac{dM}{d\log d_{va}} = \sum_i \frac{M_i}{(2\pi)^{1/2}\log\sigma_i} \exp\left[-\frac{(\log d_{va} - \log d_{va,i})^2}{2\log^2\sigma_i}\right]$$
(3)

where M_i, $d_{va,i}$, and σ_i are the mass concentration, mean diameter, and geometric standard deviation of the ith log-normal mode, and log is the base 10 logarithm (Seinfeld and Pandis, 1998). The results of the fits are presented in Table 3 and in Figs. S3 and S4 of the supplementary material (http://www.atmos-chem-phys.net/6/925/acp-6-925-sp.pdf). Fits were performed with the built-in fitting routines included the in Igor Pro 5.04 data analysis software (WaveMetrics, 2005). For organics, three log-normal modes were needed in order to produce acceptable fits. For nitrate, sulfate and ammonium, we used the sum of two modes; and for chloride only one lognormal mode was required. The data presented in Fig. 7 and Table 3 may be useful for regional and global chemical transport models, to interpret remote sensing data, as well as for other applications that need to assume or verify predictions/retrievals of chemically resolved particle size distributions.

Fig. 7. Panel **a**: Average size distributions of AMS NR-PM$_1$ species for the entire measurement period. Note the different axis scales in which the inorganic and organic distributions are plotted. Panel **b**: size distributions normalized to the same maximum so that their relative shapes can be appreciated. Panel **c**: average size distribution of organics compared to average size distribution of fragments m/z 44 and 57. Panel **d**: percent concentration of the total NR-PM$_1$ mass as a function of particle size.

Table 3. Mass concentration (M_i), median diameter ($d_{va,i}$) and geometric standard deviation (σ_i) of the modes calculated by fitting log-normal functions to the AMS size distributions in Fig. 7. Note that M_i is negative for two modes for which $\sigma_i < 1$, since $\log(\sigma_i)$ is also negative for those modes.

	M_0 (μg m^{-3})	$d_{va,0}$ (nm)	σ_0	M_1 (μg m^{-3})	$d_{va,1}$ (nm)	σ_1	M_2 (μg m^{-3})	$d_{va,2}$ (nm)	σ_2
Nitrate	3.4	437	1.8	0.17	142	1.3			
Sulfate	2.8	457	1.7	0.21	144	1.4			
Ammonium	2.0	435	1.8	0.08	132	1.3			
Organics	19.5	343	1.9	−1.13	125	0.8	−0.49	71	0.7
Chloride	0.3	345	1.8						

Comparison of the organic size distribution with the size distribution of fragments m/z 44 and 57 (indicators of OOA and HOA respectively), shown in Fig. 7c, suggests that the organic size distribution is a combination of an accumulation mode mainly composed of OOA and a wider mode of HOA, which dominates the composition of the smaller particles. This observation is in agreement with AMS studies in many urban areas including Boston (Jimenez et al., 2003a), Manchester and Edinburgh, UK (Allan et al., 2003), New York City (Canagaratna et al., 2004; Drewnick et al., 2004b), Vancouver, Canada (Alfarra et al., 2004; Boudries et al., 2004; Mozurkewich et al., 2004), Pittsburgh (Zhang et al., 2004; Zhang et al., 2005b), and Tokyo (Takegawa et al., 2005). An accumulation mode (200–800 nm) organic aerosol that is rich in the OOA mass spectral signature is found in all urban areas as well as rural and remote sites (Lee et al., 2002; Alfarra et al., 2004; Topping et al., 2004) and typically contains internally mixed organics and inorganics. Smaller organic particles that are dominated by the HOA mass spectral signature are observed in urban areas and are indicative of fresh traffic emissions (Canagaratna et al., 2004; Zhang et al., 2005b). As discussed below, the smaller organic particles in the MCMA are likely not internally mixed with inorganic species. The same conclusion was reached with the BWP
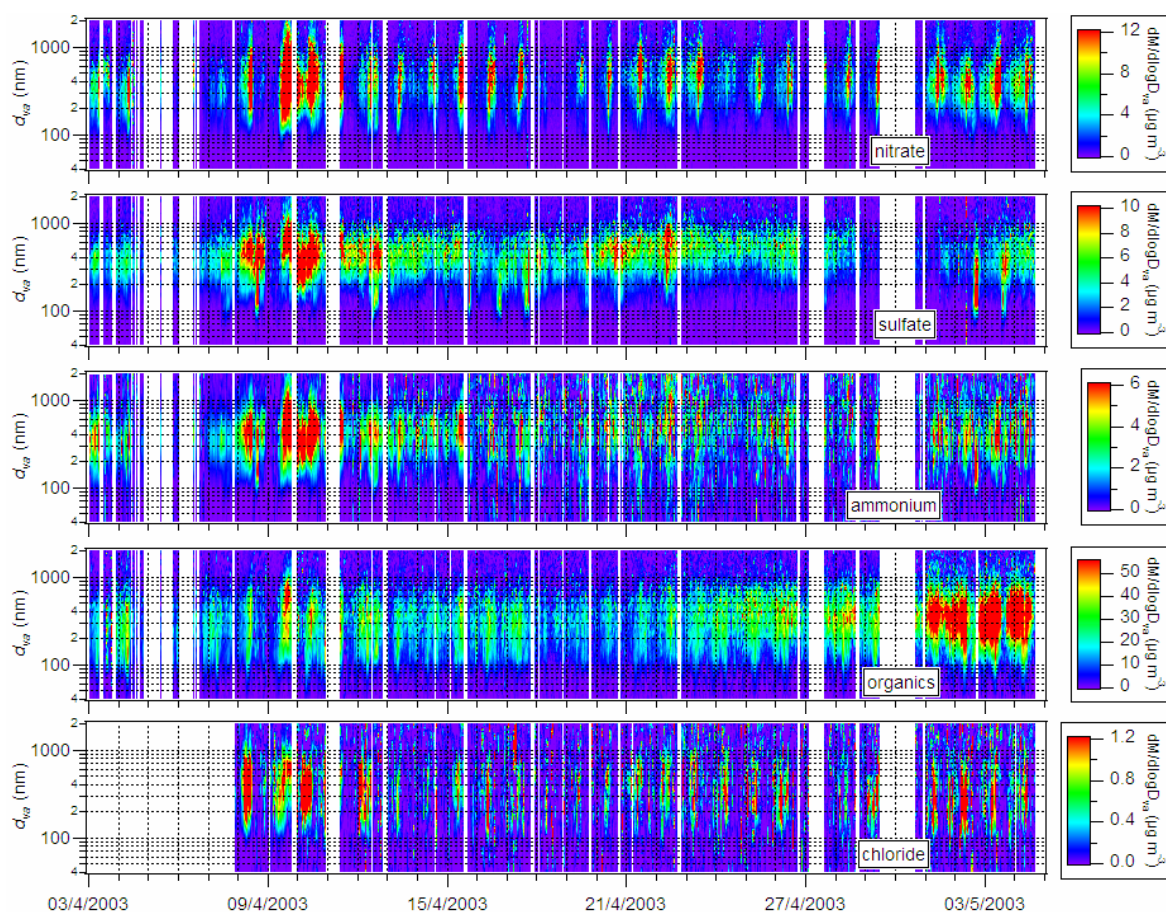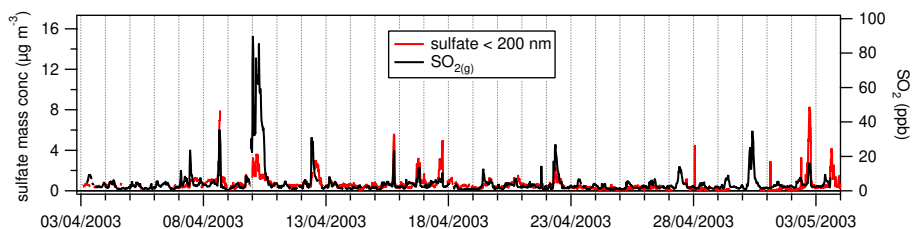
Fig. 8. Image plots of the mass concentration of the main NR-PM$_1$ species as a function of time and size for all of MCMA-2003.

used during this study (Salcedo et al., 2005). Electron microscope studies of particles collected during MCMA-2003, also found that ambient soot particles were generally internally mixed with sulfate, while fresh soot particles in vehicle exhaust were not (Johnson et al., 2005).

Figure 8 shows the variations in species size distributions as a function of time. The accumulation mode of sulfate does not show much time variation. These observations indicate that much of the sulfate observed during this campaign is formed on a regional rather than local scale (see Sect. 3.7). The nitrate image plot shows a diurnal variation in mass concentration that is consistent with local photochemical formation of this species. The similarity in size between the accumulation modes of nitrate, sulfate, and the OOA mass spectral marker (see Fig. 7) further suggests the nitrate is internally mixed with sulfate and secondary organics, as it condenses on the background aerosol. The organic size distribution time trends show that the organic accumulation mode is present throughout most of the day while the small organic particles, which as described above are likely due to fresh traffic emissions, mostly appear in the morning. The chloride size distribution shows a diurnal cycle in mass concentration

that, as discussed in Sect. 3.8, likely reflects the temperature and relative humidity dependent condensation of NH$_4$Cl onto background aerosol. Figure 8 shows that chloride size distribution usually peaks either around a d_{va} of 400 nm (i.e. from 8 April to 15 April) or around a d_{va} of around 300 nm (i.e. from 25 April to 4 May). The average chloride distribution in Fig. 7 reflects an average over both of these time periods.

Figure 8 indicates that the small particle mode of sulfate (which corresponds to the mode with median diameter 144 nm in Table 3) is only observed during a few distinct plume events. These small particle sulfate events do not correlate with analogous events in any of the other measured species and thus suggest that the small sulfate particles are externally mixed from the small organic particles. In order to investigate the sources of this mode, we integrated the mass between 20 and 200 nm for the data in Fig. 8 and obtained the time series of the mass concentration of sulfate in particles with $d_{va}<200$ nm, which is plotted in Fig. 9 together with the mixing ratio of SO$_2$ in the gas phase (measured with differential optical absorption spectroscopy – DOAS). This figure shows that the presence of a small sulfate mode was usually accompanied by plumes in sulfur dioxide, which

Fig. 9. Time series of the mass concentration of sulfate in particles with $d_{va} < 200$ nm and time series of the mixing ratio of SO_2 in the gas phase.

suggests that the origin of the smaller mode in the sulfate size distribution is the formation and growth of new particles, as was reported before by Dunn et al. (2004). In fact, the plume observed on 3 May corresponds to a particle formation event observed with a scanning mobility particle sizer (SMPS) (Dunn et al., 2004).

3.5 Ion balance

Figure 10a shows the concentration of ammonium measured during MCMA-2003 compared with the concentration of ammonium expected (NH_4^+ predicted) if all the nitrate, chloride and sulfate existed as NH_4NO_3, NH_4Cl, and $(NH_4)_2SO_4$, i.e. were completely neutralized. If this was the case, NH_4^+ predicted should be equal to NH_4^+ measured. In Fig. 10c, we show the "missing NH_4^+" (the difference between the predicted assuming NH_4NO_3, NH_4Cl, and $(NH_4)_2SO_4$ and the measured ammonium) in the aerosol. If all the nitrate, chloride and sulfate were neutralized, "missing NH_4^+" should be equal to zero. Panels a and c of Fig. 10 show that this was not always the case during MCMA-2003; for example between 7 April and 13 April predicted NH_4^+ was larger than measured NH_4^+ most of the time. Although there are other short periods where this is also the case, we focus on 7 April–13 April because of its length. For this period, we also calculated the predicted ammonium if sulfate was in the form of ammonium bisulfate (NH_4HSO_4) instead of ammonium sulfate. The result is shown in Fig. 10b. In this case, predicted vs. measured ammonium fall closer to the 1:1 line, suggesting that, during this period, the sulfate was not completely neutralized. Interestingly, this period corresponds to the highest particle sulfate concentrations measured during the campaign, as is shown in Fig. 10c.

During those periods when measured and predicted NH_4^+ do not agree, we cannot rule out the presence of organic nitrates in the condensed phase. Another possible cause of the disagreement might be the neutralization of nitric acid on soil surfaces, rather than driven by gas phase ammonia; this process has been suggested to affect the NO_y chemistry (Bauer et al., 2004; Seisel et al., 2004). However, because the periods with ammonium deficit corresponded to high sulfate concentration, while soil concentrations were similar to those during the rest of the campaign, it is more likely that

the reason for the discrepancy between measured and predicted NH_4^+ was the presence of high concentrations of sulfate which were not completely neutralized by the available gas phase ammonia.

Moya et al. (2003) reported periods of non-neutralized particles at a site in the National University Campus (UNAM), about 10 km West of CENICA, which were associated with SO_2 emissions from the Popocatepetl volcano and high RH, both conditions promoting the increase of particulate sulfate. During MCMA-2003 the volcano activity was low; however, the high sulfate events on 9, 10 and 11 April are linked with regional pollution events, driven by active photochemistry, low mixing heights and surface inversions, as well as flow from the North, where the main anthropogenic SO_2 sources are located in the Tula area (de Foy et al., 2005).

3.6 Secondary nitrate production

Ammonium nitrate is formed by the following reaction between $NH_{3(g)}$ and $HNO_{3(g)}$:

$$NH_{3(g)} + HNO_{3(g)} \longleftrightarrow NH_4NO_{3(s,aq)} \tag{4}$$

The ammonium nitrate formed can exist as a solid or in solution and, and it can dissociate back to the gas-phase reactants. The equilibrium constant of Reaction (4) is strongly dependent on the relative humidity and the temperature, and it can change by several orders of magnitude under typical atmospheric conditions (Stelson and Seinfeld, 1982).

Unfortunately, there were no continuous measurements of $HNO_{3(g)}$ at CENICA during MCMA-2003. On the other hand, NO_2 and OH in the gas phase were measured with differential optical absorption spectroscopy (DOAS) and laser-induced fluorescence (LIF), respectively (Shirley et al., 2005; Volkamer et al., 2005). With this information, the rate of the photochemical production of nitric acid can be estimated from the following reaction:

$$NO_{2(g)} + OH \cdot + M \longrightarrow M + HNO_{3(g)} \tag{5}$$
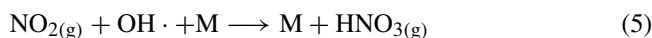
Kinetic data used for the calculation is shown in Table 4 (JPL, 2003). As reference, this table presents the calculated bimolecular rate-constant for the mean temperature and pressure conditions of the campaign (295 K, 76 kPa). However, for the following analysis, measured ambient temperature
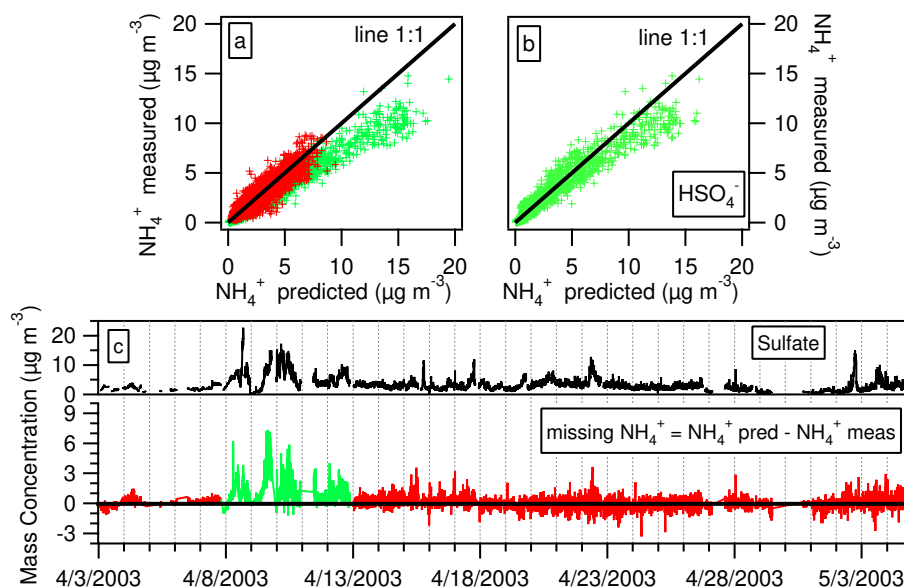
Fig. 10. Panel **a**: measured ammonium vs. predicted NH_4^+ if all nitrate, chloride, and sulfate existed as NH_4NO_3, NH_4Cl and $(NH_4)_2SO_4$. Panel **b**: measured ammonium between 8 and 13 April vs. predicted NH_4^+ if all nitrate existed as NH_4NO_3, chloride as NH_4Cl, and sulfate as $NH4HSO4$. Panel **c**: time series of sulfate and missing NH_4^+. Green color in all the panels is used to differentiate data between 8 and 13 April from the rest of the campaign (in red).

Table 4. Kinetic data used for the production rates of nitric and sulfuric acid (JPL, 2003). As reference, calculated bimolecular rate-constant for the mean temperature and pressure conditions during the campaign (295 K, 76 kPa) are presented.

$$k_o(T) = k_0^{300} \left(\frac{T}{300} \right)^{-n} \quad (\text{cm}^6 \text{ molecule}^{-2} \text{ s}^{-1})$$

$$k_\infty(T) = k_\infty^{300} \left(\frac{T}{300} \right)^{-m} \quad (\text{cm}^3 \text{ molecule}^{-1} \text{ s}^{-1})$$

$$k(T, [M]) = \left(\frac{k_o(T)[M]}{1 + k_o(T)[M]/k_\infty(T)} \right) 0.6^{\left\{ 1 + \left[\log\left(\frac{k_O(T)[M]}{k_\infty(T)} \right) \right]^2 \right\}^{-1}} \quad (\text{cm}^6 \text{ molecule}^{-2} \text{ s}^{-1})$$

	k_o^{300}	n	k_∞^{300}	m	k (295 K, 76 kPa) cm^6 molecule^{-2} s^{-1}
$OH + NO_2 \xrightarrow{M} HONO_2$	2.0×10^{-30}	3.0	2.5×10^{-11}	0	9.3×10^{-12}
$OH + SO_2 \xrightarrow{M} HOSO_2$	3.0×10^{-31}	3.3	1.5×10^{-12}	0	8.2×10^{-13}

and pressure as a function of time were used to calculate the rate constants for each data point.

Figure 11a shows the average HNO_3 diurnal production rate calculated for Reaction (5) together with the observed diurnal rate of change in particulate NO_3^- (the diurnal cycle of nitrate can be seen in Fig. 5a). Qualitatively, in the morning, particulate nitrate increases in a way that is consistent with the production of nitric acid and the partitioning of about 1/3 of it to the particulate phase. However, after 11:00 AM the nitrate concentration in particles decreases continually, while

nitric acid is still being produced. This observation can be explained by the increase in the boundary layer (BL) height and temperature and the decrease in the RH as the day progresses. Changes in the BL height can be estimated from the volume dilution factor, computed from the observed dilution of vehicular emissions of carbon monoxide[1] and shown in

---

[1] García, A., Volkamer, R., Molina, L. T., et al.: Estimation of volume dilution factor using a inert chemical tracer, in preparation, 2005.
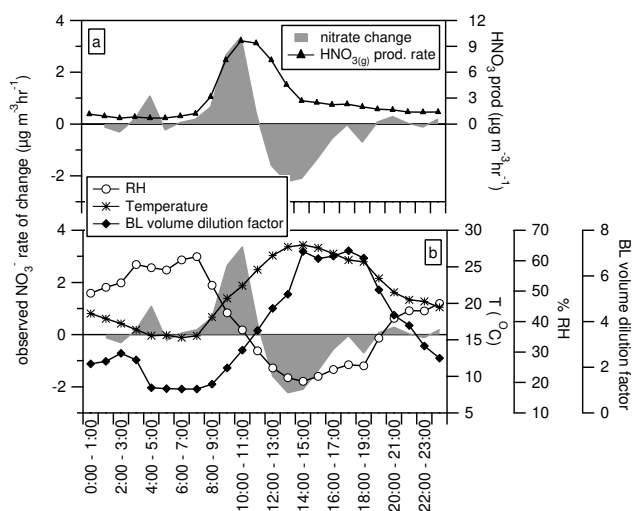
**Fig. 11.** Panel **a**: Diurnal production rate of $HNO_{3(g)}$ from Reaction (5) and observed rate of change of the mass concentration of nitrate. Panel **b**: diurnal cycles of RH, temperature and volume dilution factor of the BL.

Fig. 11b along with temperature and RH. Although, photochemical production of HNO_3 is still active after 11:00 AM, the increase in the BL height mixes the particles in the shallow morning boundary layer with air from a much larger volume where nitrate concentrations are low, and the dilution plus the increase in temperature and decrease in RH shift equilibrium (4) towards the gas phase species. These factors offset the continued HNO_3 production in the atmosphere, leading to a decrease the concentration of nitrate in the aerosol.

3.7 Secondary sulfate production

The main source of sulfate in the particles is the oxidation of SO_2 in the gas or the aqueous phase. In the gas phase, the major SO_2 oxidant is OH through the following reaction:

$$SO_{2(g)} + OH \cdot + M \longrightarrow M + HOSO_{2(g)} \qquad (6)$$
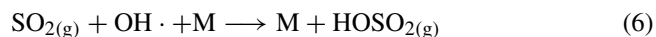
Reaction (6) is followed by fast reactions with O_2 and H_2O to finally form H_2SO_4, which has a low vapor pressure, and rapidly condenses in preexisting particles or forms new ones. We estimated the sulfuric acid production rate in the gas phase as the rate of Reaction (6) from OH and SO_2 gas phase concentrations, measured with LIF and DOAS, respectively (Shirley et al., 2005; Volkamer et al., 2005). Table 4 presents the kinetic data used (JPL, 2003). The rate-constant for the mean temperature and pressure conditions of the campaign (295 K, 76 kPa) is presented as reference. However, for the following analysis, measured ambient temperature and pressure as a function of time were used to calculate the rate constants for each data point.

Figure 12 shows average diurnal cycles of the sulfuric acid production rate from Reaction (6) together with particulate
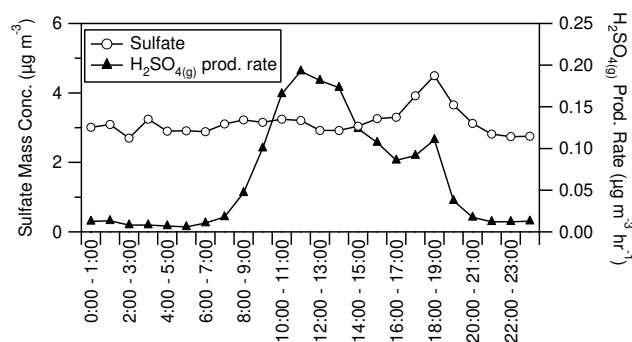

Fig. 12. Diurnal production rate of $H_2SO_{4(g)}$ from Reaction (6) and diurnal cycle of sulfate mass concentration. Averages were made over all time periods where sulfate, SO_2 and OH data was available.

sulfate concentration. In contrast with the nitric acid case, Fig. 12 does not show much correlation between the two quantities. The concentration of sulfate is relatively constant during the day, even when there is a maximum of sulfuric acid production at midday. Both quantities show a peak at 17:00–19:00; however the rate of increase of sulfate before this peak is seven times larger than what can be explained by gas-phase production, which implies that this feature is likely due to transport. In conclusion, local gas-phase sulfate production seems to be a minor player in the variations of the concentration of this species in Mexico City. Instead, processes on a regional scale seem to be the main contributors to the variations of this species.

Measurements carried out during a previous campaign at a south west location at an elevation 440 m above the average level of Mexico City suggest that high RH conditions enhance the fraction of sulfate in the aerosols due to aqueous phase SO_2 oxidation (Raga et al., 1999; Baumgardner et al., 2000; Moya et al., 2003). We tested this conclusion by comparing the concentration of sulfate in the particles and measured RH at CENICA. Figure 13 compares daily averages of both quantities during MCMA-2003, showing a very similar time trend. The insert in Fig. 13 shows a scatter plot of sulfate mass concentration and RH for four-minute data, as well as daily averages. The scatter of the four-minute data is significant (as is shown by the low r^2 of the linear correlation). However, the correlation is better between the daily averages (r^2=0.473). This is likely a consequence of the fact sulfate is produced in a regional rather than local scale. Figure 13 is in agreement with conclusions reached by Raga et al. (1999), Baumgadner et al. (2000) and Moya et al. (2003).

3.8 Chloride

The highest concentrations of chloride during MCMA-2003 were measured during the night and early morning (Fig. 7e), and large short-lived plumes of this species were often observed at these times, as shown in Fig. 14.
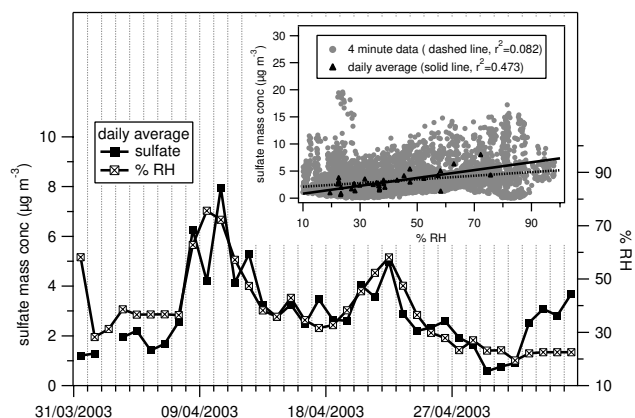
Fig. 13. Daily average of sulfate mass concentration and RH measured. Insert: scatter plot of the daily averages and 4-min data of sulfate mass concentration and RH. Linear fits for both data sets as well as the corresponding correlation coefficients are shown.
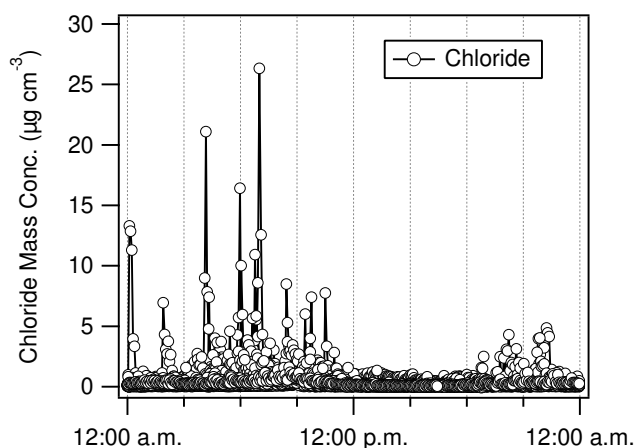
Fig. 14. Chloride mass concentration as a function of time of day for the whole campaign, with all days superimposed on top of each other.

NH_4Cl is a semivolatile solid with a partial pressure product of $P_{NH_3} \times P_{HCl} \sim 8.0 \times 10^{-17}$ atm at 25°C (Clegg et al., 1998). For comparison, the partial pressure product of NH_4NO_3 is $P_{NH_3} \times P_{HNO_3} \sim 4.4 \times 10^{-17}$ atm at 25°C; i.e. NH_4Cl is more volatile than NH_4NO_3. These facts suggest that ammonium chloride in Mexico City preferentially condenses when the favorable conditions of lower temperature and higher relative humidity are present, as it has been suggested before (SanMartini, 2004).

Figure 15 shows two chloride spikes together with ammonium and organics mass concentration. In both cases ammonium shows a spike of the same width as chloride at about half the mass concentration, which suggests that chloride is present mostly as ammonium chloride (NH_4Cl). This is the case for all the chloride plumes observed during the campaign. This salt is probably formed from the reaction be-
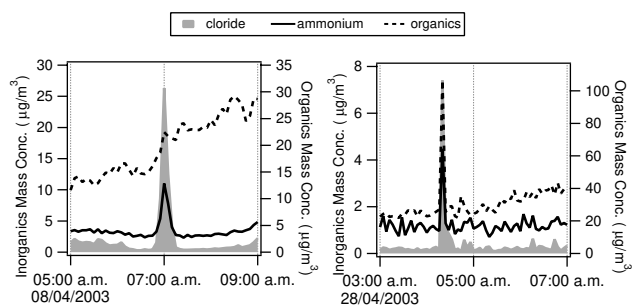
Fig. 15. Mass concentration of chloride, ammonium and organics during two chloride spike events.

tween $HCl_{(g)}$ and $NH_{3(g)}$. During the chloride spike shown in panel b, the organic concentration also increases; indicating that the same (or a collocated) source of chloride also emits organic compounds. This was observed only during two (out of about 17) of the strong plumes (with chloride concentration$>4\,\mu g\,m^{-3}$) during MCMA-2003. Possible sources of chloride without organics include drinking water and waste water treatment facilities (Tanaka et al., 2003). Refuse burning was observed to produce both chloride and organics with another AMS in mobile sampling mode, so it cannot produce the majority of the plumes observed here were a chloride spike was detected without an organic increase.

3.9 Comparison with other studies

There have been several studies on Mexico City particles, as reviewed by Raga et al. (2001) (see references therein), as well as (Raga et al., 1999; Baumgardner et al., 2000; Vega et al., 2001; Baumgardner et al., 2002; Chow et al., 2002; Vega et al., 2002; Moya et al., 2003; Vega et al., 2003; Baumgardner et al., 2004; Moya et al., 2004). However, most of them use different instrumentation and/or were carried out in locations distant from the CENICA site and/or different seasons than MCMA-2003, which makes the comparison not straightforward. The most complete published study on PM chemical properties in MCMA was the campaign "Investigación sobre Materia Particulada y Deterioro Atmosférico – Aerosol and Visibility Evaluation Research" (IMADA-AVER) (Edgerton et al., 1999; Chow et al., 2002; Vega et al., 2002), which was carried out from 23 February to 22 March 1997. During this campaign, the chemical properties of $PM_{2.5}$ and PM_{10} were measured and their temporal and spatial variations were reported at different sites in and around Mexico City. One of the sites was situated at Cerro de la Estrella (CES), located approximately 2.5 km southwest from the CENICA site. Because of the proximity of the sites and of the seasons, we compare results from IMADA-AVER at CES and MCMA in order to explore changes in the Mexico City aerosol over a period of 6 years.

During IMADA-AVER, four daily 6-hour $PM_{2.5}$ samples (0:00–6:00, 6:00–12:00, 12:00–18:00 and 18:00–24:00 h
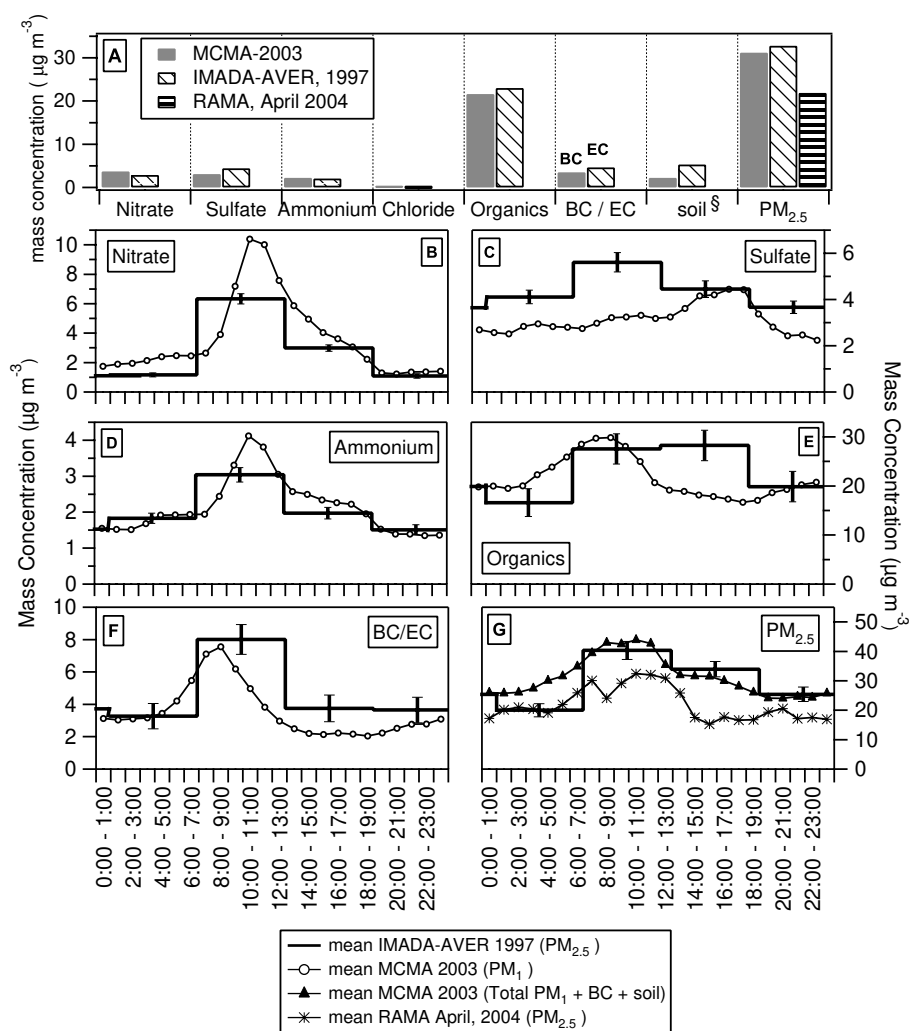
Fig. 16. Comparison of results from MCMA-2003 and IMDA-AVER at CES in February–March, 1997 (Chow et al., 2002), and report of the monitoring network in Mexico City (RAMA) during April 2004 at the Metropolitan University, campus Iztapalapa. Panel **a**: average mass concentration of species measured. Panels **b–f**: average diurnal profiles of $PM_{2.5}$ species measured during MCMA-2003 and IMADA-AVER. Panel **g**: average mass concentration of $PM_{2.5}$. All data is plotted vs. local time. Vertical lines in panels b to g represents the standard deviation of the IMADA-AVER data.

MST, 1 h behind CST) were taken daily at the CES site. The samples were analyzed for water-soluble sulfate, ammonium, nitrate, sodium and potassium; for organic and elemental carbon (OC/EC); and for 38 elements (Chow et al., 2002).

Figure 16 compares mass concentrations and diurnal cycles of $PM_{2.5}$ components reported at CES during IMADA-AVER and MCMA-2003. The IMADA-AVER nitrate is the "Total particulate nitrate" in Table 3 of Chow et al. (2002); organic mass is calculated from the organic carbon in the same table, multiplied by 1.6 in order to estimate the particulate organic mass (Turpin and Lim, 2001). Aethalometer BC during MCMA-2003 and EC during IMADA-AVER are also compared. Note, however, that care must be taken when comparing BC and EC concentrations, especially if they are performed in different times and places, because it has been

shown that estimations of BC using an aethalometer can be up to about a factor of three different than simultaneous measurements of elemental carbon (EC) using a thermal-optical method, depending on the physical and chemical characteristics of light absorbing species in the particles (Jeong et al., 2004). Soil concentration for the IMADA-AVER campaign was calculated using the method described by Malm et al. (1994) and the mass concentrations of Al, Si, Ca, Fe, and Ti reported by Chow et al. (2002). Finally, Fig. 16 compares AMS + BC + soil during MCMA-2003, total $PM_{2.5}$ during IMADA-AVER ("Mass-all days" row in Table 3 of Chow et al., 2002), and $PM_{2.5}$ during April 2004 at the campus Iztapalapa of the Metropolitan University (where CENICA is located) reported by the Air Quality Monitoring Network in Mexico City (RAMA, http://www.sma.df.gob.mx/simat/

paginabases.htm). The PM$_{2.5}$ monitoring network (TEOM at 30°C to limit evaporation losses) started its operation in 2004, hence there is no 1997 or 2003 data reported to compare with IMADA-AVER or MCMA-2003.

Panel a in Fig. 16 compares average mass concentrations, showing similar levels of all species during MCMA-2003 and IMADA-AVER. Organics were the dominant group of species during both campaigns. Nitrate was slightly higher during MCMA-2003, which may be partially due to the lower sulfate concentrations and thus reduced competition for gas-phase NH$_3$ during this campaign. The larger difference in mass concentration is observed for soil. The differences observed in Fig. 16 are probably due to differences in precipitation during both campaigns: several rain episodes were observed during MCMA-2003 campaign which would tend to reduce soil entrainment, however no rain in Mexico City was reported during IMADA-AVER (Doran et al., 1998).

Panels b–f in Fig. 16 compare the total and speciated diurnal cycles for PM$_{2.5}$ measured at CES during IMADA-AVER and at CENICA during the MCMA-2003 campaign. Organics show an earlier maximum during MCMA-2003 than during IMADA-AVER. The diurnal profile of sulfate was also slightly different during both campaigns, although in both cases this species showed lower variability with time of the day than any of the other species, again consistent with a more regional characteristic. On the other hand, diurnal profiles of nitrate, ammonium, and BC/EC were more similar between the two campaigns. PM$_{2.5}$ measurements in panel g of Fig. 16 show a similar pattern, with a significant background concentration at all times and a peak in the late morning. Since the AMS + BC + soil data compare well to collocated PM$_{2.5}$ DustTrack and TEOM during MCMA-2003, the difference between PM$_{2.5}$ during IMADA-AVER in 1997, AMS + BC + soil in 2003, and the RAMA data in 2004 indicates the range of year-to-year variability at this site, likely driven by differences in meteorology and emissions.

4 Summary

An Aerodyne Aerosol Mass Spectrometer was deployed in Mexico City as part of the MCMA-2003 field campaign. The AMS can detect non-refractory particles less than 1 μm. By combining data from the AMS with aerosol BC and soil, we were able to report speciated concentrations of PM$_{2.5}$ with a high time resolution. The estimated PM$_{2.5}$ in the Mexico City Metropolitan Area during the MCMA-2003 campaign was composed of 54.6% (σ=10%) organic compounds vs. 27.5% (σ=10%) of inorganic compounds. The inorganics were mainly ammonium nitrate, sulfate/ammonium salts, and a small amount of ammonium chloride. The Black Carbon mass concentration was about 11.0% (σ=4%) of the estimated PM$_{2.5}$, while soil represents 6.7% (σ=4%).

Organic compounds comprise the largest fraction of the Mexico City aerosol. The data suggests that the organic aerosol trends in time and size are a combination of emissions and oxidation of primary organic species in the atmosphere. The importance and complexity of this fraction of the aerosol deserves a more detailed analysis to determine the relative importance of OOA and SOA at different times and/or ambient conditions.

The speciation of the inorganic fraction of the aerosol shows that most of the time the chloride, sulfate and nitrate present were neutralized by ammonium. However, there were periods when there was not enough ammonium in particles to neutralize the chloride, sulfate and nitrate present. These periods usually corresponded to periods with high sulfate concentrations, which suggest the presence of ammonium bisulfate. The degree of neutralization of the aerosol is related to temperature, relative humidity, and most importantly the gas phase concentration of NH$_3$. Measurement of gas phase NH$_3$ and HNO$_3$, as well as an independent measurement of nitrate (such as a PILS instrument) would be helpful to determine if there are other processes affecting the ion balance such as the presence of organic nitrates in the condensed phase or the neutralization of nitric acid on soil surfaces.

Nitrate presents a diurnal cycle consistent with local photochemical production on nitric acid which reacts with ammonia to form ammonium nitrate. On the other hand, sulfate seems to be formed on a regional scale from the oxidation of SO$_2$. Sulfate concentration is enhanced during high RH conditions. Although sulfate size distribution mainly shows an accumulation mode, a small mode is observed in short-lived plume events that likely indicate recent new particle formation and growth.

The speciated NR-PM$_1$ size distributions consist of an accumulation mode in which the organic and inorganic species appear to be internally mixed. The size distributions also show smaller size modes in which inorganic and organic species are often externally mixed. This raises the question of what time and length scales are important in the evolution of these species before they eventually, if ever, reach a uniform mixing state.

Comparison of the particle measurements during MCMA-2003 with those of other studies near CENICA, shows a similar pattern of total and speciated concentrations. However some differences also exist, likely due to the variability in meteorological conditions.

References

Alfarra, M. R., Coe, H., Allan, J. D., Bower, K. N., Boudries, H., Canagaratna, M. R., Jimenez, J. L., Jayne, J. T., Garforth, A., Li, S. M., and Worsnop, D. R.: Characterization of Urban and Regional Organic Aerosols In the Lower Fraser Valley Using Two Aerodyne Aerosol Mass Spectrometers, Atmos. Environ., 38, 5745–5758, 2004.

Allan, J. D., Alfarra, M. R., Bower, K. N., Williams, P. I., Gallagher, M. W., Jimenez, J. L., McDonald, A. G., Nemitz, E., Canagaratna, M. R., Jayne, J. T., Coe, H., and Worsnop, D. R.: Quantitative sampling using an Aerodyne aerosol mass spectrometer 2. Measurements of fine particulate chemical composition in two U.K. cities, J. Geophys. Res., 108, 4099–4105, 2003.

Allan, J. D., Bower, K. N., Coe, H., Boudries, H., Jayne, J. T., Canagaratna, M. R., Millet, D. B., Goldstein, A. H., Quinn, P. K., Weber, R. J., and Worsnop, D. R.: Submicron aerosol composition at Trinidad Head, CA during ITCT 2K2, its relationship with gas phase volatile organic carbon and assessment of instrument performance, J. Geophys. Res., 109, D23524, doi:10.1029/2003JD004208, 2004.

Bahreini, R., Keywood, M. D., Ng, N. L., Varutbangkul, V., Gao, S., Flagan, R. C., Seinfeld, J. H., Worsnop, D. R., and Jimenez, J. L.: Measurements of Secondary Organic Aerosol (SOA) from oxidation of cycloalkenes, terpenes, and m-xylene using an Aerodyne Aerosol Mass Spectrometer, Environ. Sci. Technol., 39, 5674–5688, doi:10.1021/es048061a, 2005.

Baron, P. A. and Willeke, K.: Aerosol Measurement: Principles, Techniques, and Applications, Wiley-Interscience, Hoboken, NH, 2001.

Barth, M. C. and Church, A. T.: Regional and global distributions and lifetimes of sulfate aerosols from Mexico City and southeast China, J. Geophys. Res., 104, 30 231–30 239, 1999.

Bauer, S. E., Balkanski, Y., Schulz, M., and Hauglustaine, D. A.: Global modeling of heterogeneous chemistry on mineral aerosol surfaces: Influence on tropospheric ozone chemistry and comparison to observations, J. Geophys. Res., 109, D02304, doi:10.1029/2003JD003868, 2004.

Baumgardner, D., Raga, G. B., Kok, G., Ogren, J., Rosas, I., Báez, A., and Novakov, T.: On the evolution of aerosol properties at a mountain sire above Mexico City, J. Geophys. Res., 105, 22 243–22 253, 2000.

Baumgardner, D., Raga, G. B., Peralta, O., Rosas, I., Castro, T., Kuhlbusch, T., John, A., and Petzold, A.: Diagnosing black carbon trends in large urban areas using carbon monoxide measurements, J. Geophys. Res., 107, 8342, doi:10.1029/2001JD000626, 2002.

Baumgardner, D., Raga, G. B., and Muhlia, A.: Evidence for the formation of CCN by photochemical processes in Mexico City, Atmos. Environ., 38, 357–367, 2004.

Boudries, H., Canagaratna, M. R., Jayne, J. T., Alfarra, M. R., Allan, J. D., Bower, K. N., Coe, H., Pryor, S. C., Jimenez, J. L., Brook, J. R., Li, S., and Worsnop, D. R.: Chemical and Physical processes controlling the distribution of Aerosols in the Lower Fraser Valley, Canada, during the PACIFIC 2001 field campaign, Atmos. Environ., 38, 5759–5774, 2004.

Calderon-Garciduenas, L., Mora-Tiscareno, A., Fordham, L. A., Valencia-Salazar, G., Chung, C. J., Rodriguez-Alcaraz, A., Paredes, R., Variakojis, D., Villarreal-Calderon, A., Flores-Camacho, L., Antunez-Solis, A., Henriquez-Roldan, C., and Hazucha, M. J.: Respiratory damage in children exposed to urban pollution., Pediat. Pulm, 36, 148–161, 2003.

Canagaratna, M. R., Jayne, J. T., Ghertner, D. A., Herndon, S., Shi, Q., Jimenez, J. L., Silva, P. J., Williams, P. I., Lanni, T., Drewnick, F., Demerjian, K. L., Kolb, C. E., and Worsnop, D. R.: Chase Studies of Particulate Emissions from in-use New York City Vehicles, Aerosol Sci. Technol., 38, 555–573, 2004.

Chow, J. C., Watson, J. G., Edgerton, S. A., and Vega, E.: Chemical composition of PM$_{2.5}$ and PM$_{10}$ in Mexico City during winter 1997, Sci. Total Environ., 287, 177–201, 2002.

Clegg, S. L., Brimblecombe, P., and Wexler, A. S.: A thermodynamic model of the system $H^+ - NH_4^+ - Na^+ - SO_4^{2-} - NO_3^- - Cl^- - H_2O$ at 298.15 K, J. Phys. Chem. A, 102, 2155–2171, 1998.

de Foy, B., Caetano, E., Magaña, V., Zitácuaro, A., Cárdenas, B., Retama, A., Ramos, R., Molina, L. T., and Molina, M. J.: Mexico City basin wind circulation during the MCMA-2003 field campaign, Atmos. Chem. Phys., 5, 2267–2288, 2005.

DeCarlo, P. F., Slowik, J. G., Worsnop, D. R., Davidovits, P., and Jimenez, J. L.: Particle Morphology and Density Characterization by Combined Mobility and Aerodynamic Diameter Measurements. Part 1: Theory, Aerosol Sci. Technol., 38, 1185–1205, doi:10.1080/027868290903907, 2004.

Doran, J. C., Abbott, S., Archuleta, J., Bian, X., Chow, J., Coulter, R. L., de Wekker, S. F., Edgerton, S., Elliott, S., Fernandez, A., Fast, J. D., Hubbe, J. M., King, C., Langley, D., Leach, J., Lee, J. T., Martin, T. J., Martinez, D., Martinez, J. L., Mercado, G., Mora, V., Mulhearn, M., Pena, J. L., Petty, R., Porch, W., et al.:

The IMADA-AVER Boundary Layer Experiment in the Mexico City Area, Bull. Am. Meteorol. Soc., 79, 2497–2508, 1998.

Drewnick, F., Schwab, J. J., Jayne, J. T., Canagaratna, M. R., Worsnop, D. R., and Demerjian, K. L.: Measurement of Ambient Aerosol Composition During the PMTACS-NY 2001 Using an Aerosol Mass Spectrometer. Part I: Mass concentrations, Aerosol Sci. Technol., 38, 92–103, doi:10.1080/02786820390229507, 2004a.

Drewnick, F., Jayne, J. T., Canagaratna, M. R., Worsnop, D. R., and Demerjian, K. L.: Measurement of Ambient Aerosol Composition During the PMTACS-NY 2001 Using an Aerosol Mass Spectrometer. Part II: Chemically Speciated Mass Distributions, Aerosol Sci. Technol., 38, 104–117, 2004b.

Dunn, M. J., Jimenez, J. L., Baumgardner, D., Castro, T., Mc-Murry, P. H., and Smith, J. N.: Measurements of Mexico City nanoparticle size distributions: Observations of new particle formation and growth, Geophys. Res. Lett., 31, L10102, doi:10.1029/2004GL019483, 2004.

Edgerton, S. A., Bian, X., Doran, J. C., Fast, J. D., Hubbe, J. M., Malone, E. L., Shaw, W. J., Whiteman, C. D., Zhong, S., Arriaga, J. L., Ortiz, E., Ruiz, M., Sosa, G., Vega, E., Limón, T., Guzmán, F., Archuleta, J., Bossert, J. E., Elliot, S. M., Lee, J. T., McNair, L. A., Chow, J. C., Coutler, R. L., Doskey, P. V., Gaffney, J. S., et al.: Particulate air pollution in Mexico City: a collaborative research project, J. Air. Waste Manage., 49, 1221–1229, 1999.

Gold, D. R., Damokosh, A., Pope, C. A., Dockery, D. W., McDonnell, W. F., Serrano, P., Retama, A., and Castillejos, M.: Particulate and ozone pollutant effects on the respiratory function of children in southwest Mexico City, Epidemiology, 10, 8–16, 1999.

Hansen, A. D. A., Rosen, H., and Novakov, T.: Real-time measurement of the absorption coefficient of aerosol particles, Appl. Opt., 21, 3060–3062, 1982.

Heberlein, J., Postel, O., Girshick, S., McMurry, P., Gerberich, W., Iordanoglou, D., F. Di Fonzo, Neumann, D., Gidwani, A., Fan, M., and Tymiak, N.: Thermal plasma deposition of nanophase hard coatings, Surf. Coat. Technol., 142, 265–271, 2001.

Hinds, W. C.: Aerosol technology; properties behavior, and measurement of airborne particles, John Wiley and Sons, USA, 1999.

Hogrefe, O., Schwab, J. J., Drewnick, F., Lala, G. G., Peters, S., Demerjian, K. L., Rhoads, K., Felton, H. D., Rattigan, O. V., Husain, L., and Dutkiewicz, V. A.: Semicontinuous $PM_{2.5}$ Sulfate and Nitrate Measurements at an Urban and a Rural Location in New York: PMTACS-NY Summer 2001 and 2002 Campaigns, J. Air. Waste Manage., 54, 1040–1060, 2004.

Huffman, J. A., Jayne, J. T., Drewnick, F., Aiken, A. C., Onasch, T., Worsnop, D. R., and Jimenez, J. L.: Design, Modeling, Optimization, and Experimental Tests of a Particle Beam Width Probe for the Aerodyne Aerosol Mass Spectrometer, Aerosol Sci. Technol., 39, 1143–1163, 2005.

INEGI: Tabulados Básicos. Estados Unidos Mexicanos. XII Censo General de Población y Vivienda, 2000, Instituto Nacional de Estadística, Geografía e Informática, Aguascalientes, 2001.

Jayne, J. T., Leard, D. C., Zhang, X., Davidovits, P., Smith, K. A., Kolb, C. E., and Worsnop, D. R.: Development of an Aerosol Mass Spectrometer for Size and Composition Analysis of Submicron Particles, Aerosol Sci. Technol., 33, 49–70, 2000.

Jeong, C.-H., Hopke, P. K., Kim, E., and Lee, D.-W.: The comparison between thermal-optical transmittance elemental carbon and Aethalometer black carbon measured at multiple monitoring sites, Atmos. Environ., 38, 5193–5204, 2004.

Jimenez, J. L., Jayne, J. T., Shi, Q., Kolb, C. E., Worsnop, D. R., Yourshaw, I., Seinfeld, J. H., Flagan, R. C., Zhang, X., Smith, K. A., Morris, J., and Davidovits, P.: Ambient aerosol sampling using the Aerodyne Aerosol Mass Spectrometer, J. Geophys. Res., 108, 8425, doi:10.1029/2001JD001213, 2003a.

Jimenez, J. L., Bahreini, R., Cocker, D. R., Zhuang, H., Varutbangkul, V., Flagan, R. C., Seinfeld, J. H., O'Dowd, C. D., and Hoffmann, T.: New particle formation from photooxidation of diiodomethane (CH_2I_2), J. Geophys. Res., 108, 4318, doi:10.1029/2002JD002452, 2003b.

Jimenez, J. L., Bahreini, R., Cocker, D. R., Zhuang, H., Varutbangkul, V., Flagan, R. C., Seinfeld, J. H., O'Dowd, C. D., and Hoffmann, T.: Correction to "New particle formation from photooxidation of diiodomethane (CH_2I_2)", J. Geophys. Res., 108, 4733, doi:10.1029/2003JD004249, 2003c.

Johnson, K. S., Zuberi, B., Molina, L. T., Molina, M. J., Iedema, M. J., Cowin, J. P., Gaspar, D. J., Wang, C., and Laskin, A.: Processing of soot in an urban environment: case study from the Mexico City Metropolitan Area, Atmos. Chem. Phys., 5, 3033–3043, 2005.

Johnson, K., de Foy, B., Zuberi, B., Molina, L., Molina, M., Xie, Y., Laskin, A., and Shutthanandan V.: Aerosol composition and source apportionment in the Mexico City Metropolitan Area with PIXE/PESA/STIM and multivariate analysis, Atmos. Chem. Phys. Dicuss., accepted, 2006.

JPL: Chemical Kinetics and Photochemical Data for Use in Atmospheric Studies, Evaluation Number 14, Jet Propulsion Laboratory, Pasadena, CA, 2003.

Katrib, Y., Martin, S. T., Rudich, Y., Davidovits, P., Jayne, J. T., and Worsnop, D. R.: Density Changes of Aerosol Particles as a Result of Chemical Reaction, Atmos. Chemi. Phys., 5, 275–291, 2005.

Lee, S.-H., Murphy, D. M., Thomson, D. S., and Middlebrook, A. M.: Chemical components of single particles measured with Particle Analysis by Laser Mass Spectrometry (PALMS) during the Atlanta SuperSite Project: Focus on organic/sulfate, lead, soot, and mineral particles, J. Geophys. Res., 107, 4003, doi:10.1029/2000JD000011, 2002.

Lide, D. R.: CRC Handbook of Chemistry and Physics, CRC Press Inc, USA, 1991.

Malm, W. C., Sisler, J. F., Huffman, D., Eldred, R. A., and Cahil, T. A.: Spatial and seasonal trends in particle concentration and optical extinction in the United States, J. Geophys. Res., 99, 1347–11370, 1994.

Marley, N. A., Gaffney, J. S., Baird, J. C., Blazer, C. A., Drayton, P. J., and Frederick, J. E.: The determination of scattering and absorption coefficients of size-fractionated aerosols for radiative transfer calculations, Aerosol Sci. Technol., 34, 535–549, 2001.

Maxwell, J. A., Campbell, J. L., and Teesdale, W. J.: The Guelph-PIXE software package-II, Nucl. Instrum. Methods Phys. Res. B, 3, 407–421, 1995.

Molina, L. T., and Molina, M. J.:Cleaning the air: a comparative overview, in: Air Quality in the Mexico Megacity. An Integrated Assessment, edited by: Molina, L. T. and Molina, M. J., Kluwer Academic, Netherlands, 2002.

Moya, M., Castro, T., Zepeda, M., and Baez, A.: Characterization of size-differentiated inorganic composition of aerosols in Mex-

ico City, Atmos. Environ., 37, 3581–3591, 2003.

Moya, M., Grutter, M., and Báez, A.: Diurnal variability of size-differentiated inorganic aerosols and their gas-phase precursors during January and February of 2003 near downtown Mexico City, Atmos. Environ., 38, 5651–5661, 2004.

Mozurkewich, M., Chan, T.-W., Aklilu, Y.-A., and Verheggen, B.: Aerosol particle size distributions in the lower Fraser Valley: evidence for particle nucleation and growth, Atmos. Chem. Phys., 4, 1047–1062, 2004.

Murphy, D. M., Thomson, D. S., Kaluzhny, M., Marti, J. J., and Weber, R. J.: Aerosol characteristics at Idaho Hill during the OH Photochemistry Experiment, J. Geophys. Res., 102, 6325–6330, 1997.

Osornio-Vargas, A. R., Bonner, J. C., Alfaro-Moreno, E., Martinez, L., Garcia-Cuellar, C., Rosales, S. P. D., Miranda, J., and Rosas, I.: Proinflammatory and cytotoxic effects of Mexico City air pollution particulate matter in vitro are dependent on particle size and composition, Environ. Health Perspect., 111, 1289–1293, 2003.

Park, K., Kittelson, D. B., Zachariah, M. R., and McMurry, P. H.: Measurement of Inherent Material Density of Nanoparticle Agglomerates, J. Nanopart. Res., 6, 267–272, 2004.

Raga, G. B., Kok, G. L., Baumgardner, D., Báez, A., and Rosas, I.: Evidence for volcanic influence on Mexico City aerosols, Geophys Res. Lett., 26, 1149–1152, 1999.

Raga, G. B., Baumgardner, D., Castro, T., Martinez-Arroyo, A., and Navarro-Gonzalez, R.: Mexico City air quality: a qualitative review of gas and aerosol measurements (1960–2000), Atmos. Environ., 35, 4041–4058, 2001.

Salcedo, D., Dzepina, K., Onasch, T. B., Canagaratna, M. R., Huffman, J. A., DeCarlo, P. F., Jayne, J. T., Mortimer, P., Worsnop, D. R., Kolb, C. E., Johnson, K. S., Zuberi, B., Marr, L. C., Molina, L. T., Molina, M. J., Cardenas, B., Bernabé, R. M., Márquez, C., Gaffney, J. S., Marley, N. A., Laskin, A., Shutthanandan, V., and Jimenez, J. L.: Characterization of ambient aerosols in Mexico City during the MCMA-2003 campaign with aerosol mass spectrometry. Part I: quantification, shape-related collection efficiency, and comparison with collocated instruments, Atmos. Chem. Phys. Discuss., 5, 4143–4182, 2005.

SanMartini, F. M.: Decision Support Tools for Urban Air Quality Management. Ph.D. Thesis, Massachusetts Institute of Technology, Cambridge, MA, 2004.

Schlenker, J. C., Malinowski, A., Martin, S. T., Hung, H. M., and Rudich, Y.: Crystals formed at 293 K by aqueous sulfate-nitrate-ammonium-proton aerosol particles, J. Phys. Chem. A, 108, 9375–9383, 2004.

Seinfeld, J. H. and Pandis, S. N.: Atmospheric chemistry and physics, From air pollution to climate change, John Wiley and Sons, USA, 1998.

Seisel, S., Borensen, C., Vogt, R., and Zellner, R.: The heterogeneous reaction of HNO_3 on mineral dust and gamma-alumina surfaces: a combined Knudsen cell and DRIFTS study, Phys. Chem. Chem. Phys., 6, 5498–5508, doi:10.1039/b410793d, 2004.

Shirley, T. R., Brune, W. H., Ren, X., Mao, J., Lesher, R., Cardenas, B., Volkamer, R., Molina, L. T., Molina, M. J., Lamb, B., Velasco, E., Jobson, T., and Alexander, M.: Atmospheric oxidation in the Mexico City Metropolitan Area (MCMA) during April 2003, Atmos. Chem. Phys. Discuss., 5, 6041–6076, 2005.

Shutthanandan, V., Thevuthasan, S., Disselkamp, R., Stroud, A., Cavanagh, A., Adams, E. M., Baer, D. R., Barrie, L. A., Cliff, S. S., Jimenez-Cruz, M., and Cahill, T. A.: Development of PIXE, PESA and transmission ion microscopy capability to measure aerosols by size and time, Nucl. Instrum. Methods Phys. Res. B, 189, 284–288, 2002.

Slowik, J. G., Stainken, K., Davidovits, P., Williams, L. R., Jayne, J. T., Kolb, C. E., Worsnop, D. R., Rudich, Y., DeCarlo, P., and Jimenez, J. L.: Particle Morphology and Density Characterization by Combined Mobility and Aerodynamic Diameter Measurements. Part 2: Application to combustion Generated Soot Aerosols as a Function of Fuel Equivalence Ratio, Aerosol Sci. Technol., 38, 1206–1222, 2004.

SMADF: Inventario de Emisiones a la atmósfera. Zona Metropolitana del Valle de Mexico, 2000, Secretaria del Medio Ambiente del Distrito Federal, Mexico, 2002.

SMADF: Informe del Estado de la Calidad del Aire y Tendencias para la Zona Metropolitana del Valle de México – 2002, Secretaria del Medio Ambiente del Distrito Federal, Mexico, 2003.

Stelson, A. W. and Seinfeld, J. H.: Relative humidity and temperature dependence of the ammonium nitrate dissociation constant, Atmos. Environ., 16, 983–993, 1982.

Takegawa, N., Kondo, Y., Komazaki, Y., Miyazaki, Y., Miyakawa, T., Jimenez, J. L., Jayne, J. T., Worsnop, D. R., Allan, J. D., and Weber, R. J.: Characterization of an Aerodyne Aerosol Mass Spectrometer (AMS): Intercomparison with Other Aerosol Instruments, Aerosol Sci. Technol., 39, 760–770, 2005.

Tanaka, P. L., Riemer, D. D., Chang, S., Yarwood, G., McDonald-Buller, E. C., Apel, E. C., Orlando, J. J., Silva, P. J., Jimenez, J. L., Canagaratna, M. R., Neece, J. D., Mullins, C. B., and Allen, D. T.: Direct evidence for chlorine-enhanced urban ozone formation in Houston, Texas, Atmos. Environ., 37, 1393–1400, 2003.

Topping, D., Coe, H., McFiggans, G., Burgess, R., Allan, J. D., Alfarra, M. R., Bower, K. N., Choularton, T. W., Decesari, S., and Facchini, M. C.: Aerosol chemical characteristics from sampling conducted on the Island of Jeju, Korea during ACE Asia, Atmos. Environ., 38, 2111–2123, 2004.

TSI: DUSTTRAK Aerosol Monitor Theory of Operation, TSI incorporated, St. Paul, MN, 2004.

Turpin, B. J. and Lim, H.-J.: Species Contributions to $PM_{2.5}$ Mass Concentrations: Revisiting Common Assumptions for Estimating Organic Mass, Aerosol Sci. Technol., 35, 602–610, 2001.

Vega, E., Mugica, V., Reyes, E., Sánchez, G., Chow, J. C., and Watson, J. G.: Chemical composition of fugitive dust emitters in Mexico City, Atmos. Environ., 35, 4033–4403, 2001.

Vega, E., Reyes, E., Sanchez, G., Ortiz, E., Ruiz, M., Chow, J. C., Watson, J., and Edgerton, S.: Basic statistics of $PM_{2.5}$ and PM_{10} in the atmosphere of Mexico City, Sci. Total Environ., 287, 167–176, 2002.

Vega, E., Reyes, E., Wellens, A., Sánchez, G., Chow, J. C., and Watson, J. G.: Comparison of continuous and filter based mass measurements in Mexico City, Atmos. Environ., 37, 2783–2793, 2003.

Volkamer, R., Molina, L. T., Molina, M. J., Shirley, T., and Brune, W. H.: DOAS measurement of glyoxal as an indicator for fast VOC chemistry in urban air, Geophys Res. Lett., 32, L08806, doi:10.1029/2005GL022616, 2005.

WaveMetrics: IGOR Pro. V5.0, User's Guide, WaveMetrics, Inc., USA, 2005.

Zhang, Q., Stanier, C. O., Canagaratna, M. R., Jayne, J. T., Worsnop, D. R., Pandis, S. N., and Jimenez, J. L.: Insights into the Chemistry of New Particle Formation and Growth Events in Pittsburgh Based on Aerosol Mass Spectrometry, Environ. Sci. Technol., 38, 4797–4809, 2004.

Zhang, Q., Alfarra, M. R., Worsnop, D. R., Allan, J. D., Coe, H., Canagaratna, M. R., and Jimenez, J. L.: Deconvolution and Quantification of Hydrocarbon-like and Oxygenated Organic Aerosols Based on Aerosol Mass Spectrometry, Environ. Sci. Technol., 39, 4938–4952, doi:10.1021/es048568l, 2005a.

Zhang, Q., Canagaratna, M. R., Jayne, J. T., Worsnop, D. R., and Jimenez, J. L.: Time and Size-Resolved Chemical Composition of Submicron Particles in Pittsburgh. Implications for Aerosol Sources and Processes, J. Geophys. Res., 110, D07S09, doi:10.1029/2004JD004649, 2005b.

Zhang, Q., Worsnop, D. R., Canagaratna, M. R., and Jimenez, J. L.: Hydrocarbon-like and oxygenated organic aerosols in Pittsburgh: insights into sources and processes of organic aerosols, Atmos. Chem. Phys. 5, 3289–3311, 2005c.